Science of the Total Environment 782 (2021) 146841

Contents lists available at ScienceDirect

Science of the Total Environment

journal homepage: www.elsevier.com/locate/scitotenv

Coupled hydrological and geochemical impacts of wildfire in peatland-dominated regions of discontinuous permafrost

Caren Ackley [a], Suzanne E. Tank [b], Kristine M. Haynes [a,*], Fereidoun Rezanezhad [c], Colin McCarter [d], William L. Quinton [a]

[a] Cold Regions Research Centre, Wilfrid Laurier University, Waterloo, ON, Canada
[b] Department of Biological Sciences, University of Alberta, Edmonton, AB, Canada
[c] Ecohydrology Research Group, Department of Earth and Environmental Sciences and Water Institute, University of Waterloo, Waterloo, ON, Canada
[d] Department of Physical and Environmental Sciences, University of Toronto Scarborough, Toronto, ON, Canada

HIGHLIGHTS

- Discontinuous permafrost low-severity wildfire resulted in surface peat singeing.
- Hydrology, geochemistry, peat properties, permafrost dynamics all impacted by burn.
- Fire produces uniformly lowered frost table with limited depressional storage.
- Peat physical, hydraulic properties altered post-fire with ash translocation.
- Fire triggers elevated pore water solute, organic matter, mercury concentrations.

GRAPHICAL ABSTRACT

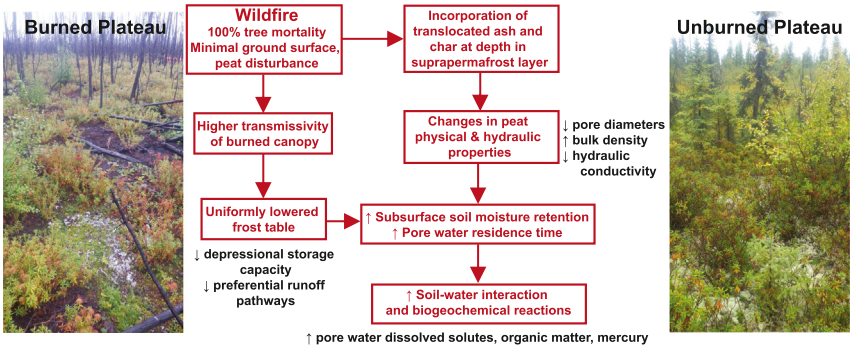

ARTICLE INFO

Article history:
Received 11 September 2020
Received in revised form 24 March 2021
Accepted 25 March 2021
Available online 30 March 2021

Editor: Paulo Pereira

Keywords:
Subarctic
Snowmelt
Ground thaw
Peat hydraulics
Ash translocation
Residence time

ABSTRACT

Naturally-ignited wildfires are increasing in frequency and severity in northern regions, contributing to rapid permafrost thaw-induced landscape change driven by climate warming. Low-severity wildfires typically result in minor organic matter loss. The impacts of such fires on the hydrological and geochemical dynamics of peat plateau-wetland complexes have not been examined. In 2014, a low-severity wildfire, with minimal ground surface damage, burned approximately one-half of a 5 ha permafrost plateau in the wetland-dominated landscape of the Scotty Creek watershed, Northwest Territories, Canada, in the discontinuous permafrost zone. In March 2016, hydrometeorological and permafrost conditions on the burned and unaffected plateaus were monitored including snowpack characteristics and surface energy dynamics. Pore water samples were collected from the saturated layer as thaw progressed throughout the growing season on the burned and unaffected plateaus. Repeated probing of the frost table depth was coupled with laboratory analyses of peat physical and hydraulic characteristics performed on peat cores collected from the top 20 cm of the ground surface in the burned and unaffected plots. The higher transmissivity of the burned forest canopy accelerated snowmelt promoting earlier onset of the thawing season and increased the ground heat flux to melt ground ice. Wildfire increased the thickness of the supra-permafrost layer, including the active layer and talik, resulting in a more uniform subsurface with limited depressional storage capacity and reduced preferential runoff flowpaths across the burned plateau. The incorporation of ash and char into the peat matrix reduced pore diameters, promoting greater subsurface soil moisture retention and longer pore water residence times ultimately providing greater opportunity for soil-water interaction and biogeochemical reactions. Consequently, pore water showed elevated dissolved solutes,

* Corresponding author at: Cold Regions Research Centre, Wilfrid Laurier University, 75 University Ave. West, Waterloo, Ontario N2L 3C5, Canada.
E-mail address: khaynes@wlu.ca (K.M. Haynes).

https://doi.org/10.1016/j.scitotenv.2021.146841

dissolved organic matter and mercury concentrations in the burned site. Low-severity wildfires have the potential to trigger a series of complex, inter-related hydrological, thermal and biogeochemical processes and feedbacks.

1. Introduction

Rapidly warming temperatures have been observed throughout the circumpolar region of the Northern Hemisphere (Richter-Menge et al., 2017), triggering broad-scale permafrost loss and subsequent biophysical and hydrological changes in the form and function of this mosaicked subarctic landscape sensitive to climate warming (Kwong and Gan, 1994; Jorgenson and Osterkamp, 2005; Quinton et al., 2019). Mean annual air temperatures have steadily risen throughout northwestern Canada over the last half century (Environment Canada, 2020), and consequently, changed the ground and permafrost temperatures (Kokelj et al., 2017; Holloway et al., 2020), the rates of permafrost thaw (Jorgenson et al., 2010; Brown et al., 2015), and the frequency and severity of wildfires (Wotton et al., 2010; Koch et al., 2014; Gibson et al., 2018). In the southern Taiga Plains ecoregion, permafrost is discontinuous (Heginbottom et al., 1995; Smith et al., 2010) and concentrated into peatland-dominated lowlands (Kwong and Gan, 1994; Holloway and Lewkowicz, 2020) where the landscape is largely composed of peat plateaus and collapse scar wetlands clustered into distinct "plateau-wetland complexes" and separated by channel fens (Quinton et al., 2019). This landscape is highly juxtaposed since the plateaus are tree-covered and overlie permafrost, while the adjacent wetlands (collapse scars and fens) are treeless and permafrost-free (Zoltai and Tarnocai, 1975; Robinson, 2002). The permafrost below the plateaus is ice-rich, relatively thin (*ca.* 10 m) and typically at or very near the temperature of the freezing point depression (Connon et al., 2018). As such, much of the permafrost of the southern Taiga Plains is in a state of disequilibrium with the current climate (Helbig et al., 2016), and therefore particularly susceptible to thaw resulting from climate warming and wildfires, two of its major drivers (Brown et al., 2015). In the southern Taiga Plains, Gibson et al. (2018) reported that wildfire is directly responsible for ~25% of all thermokarst wetland expansion over the 30 year period ending in 2018, suggesting that the area of wildfire-induced permafrost thaw is of the same order of magnitude as the area of climate warming-induced permafrost thaw as demonstrated by Connon et al. (2014). There is compelling evidence that wildfires in this and other subarctic and boreal regions of North America as well as Russia are increasing in both frequency and magnitude due to climate warming (Kasischke et al., 2010; de Groot et al., 2013; Wotton et al., 2017; Hanes et al., 2019), with a 50% increase in fire occurrence projected by the end of the century (Flannigan et al., 2009).

Recent studies on the hydrology of plateau-wetland complexes provide new insights into how permafrost thaw affects their runoff processes and pathways (Connon et al., 2014) and the flux and storage of water (Haynes et al., 2018) and solutes (Gordon et al., 2016). Prior to permafrost thaw, the ground surface of a plateau rises roughly 1 m above the surface of the surrounding wetlands, so that water flows from plateaus to wetlands. The very high permeability of the near surface peat precludes overland flow on plateaus except in limited cases where the active layer is saturated with ice and/or water. The predominant runoff pathway is therefore through the active layer, specifically through the saturated layer between the water table and the underlying, relatively impermeable frost table (Wright et al., 2009). The horizontal hydraulic conductivity (K_{sat}) of the peat comprising the active layer is uniformly high in the upper and low in the lower regions of the profile, but separated by a 0.2 to 0.3 m transition zone over which K_{sat} can decrease by 3 to 4 orders of magnitude with depth (Quinton et al., 2008). As the active layer thaws each year, the frost table and overlying water table descend through the wetted profile; the rate of subsurface runoff through the saturated layer therefore decreases. However, since the drainable porosity of the peat within the active layer can decrease from ~0.6 (as a proportion of total soil volume) in the upper 0.1 m to ~0.05 at depths below 0.3 m (Quinton and Hayashi, 2005), plateaus can generate a rapid hydraulic response to rain events, even with the water table at its maximum annual depth (Wright et al., 2009; Quinton et al., 2019).

Since the elevation of the permafrost table underlying plateaus is greater than the water table elevation of their adjacent wetlands, plateaus function as 'permafrost dams' by preventing flow between the wetlands on opposing sides of a plateau. As a result, much of the wetland area within plateau-wetland complexes is hydrologically-isolated from the basin drainage network of channel fens (Connon et al., 2014). However, permafrost thaw has greatly reduced the proportion of plateau-wetland complexes occupied by hydrologically-isolated wetlands (Haynes et al., 2018). Such thaw is driven by horizontal conduction and advection from plateau margins, and vertical heat flows from the plateau ground surface (Walvoord and Kurylyk, 2016). If thaw lowers the permafrost table to a depth below that of the water table in the adjacent wetlands, then the plateau can no longer function as a dam, and as a result, it will conduct flow horizontally through its active layer from one side of the plateau to the other until the hydraulic gradient between the opposing sides is reduced to zero (Connon et al., 2018).

In a stable climate and in the absence of disturbance by wildfire, the depth to the permafrost table fluctuates within a transient zone over sub-decadal to centennial time scales (Shur et al., 2005). In contrast to such fluctuations, climate warming can drive a persistent increase in the depth to the permafrost table (Camill, 2005; Smith et al., 2010). In concert with the ecohydrological and permafrost characteristics of the landscape, climate plays a critical role in the trajectory of the post-fire landscape. In a stable climate, permafrost returns to its pre-fire condition after 3 to 4 decades (Gibson et al., 2018), while in a warming climate where permafrost is already thawing, fire can have a compounding affect that accelerates the existing thaw rates (Jorgenson et al., 2010; Nossov et al., 2013; Brown et al., 2015). As the permafrost table lowers, it will reach a critical depth beyond which the overlying peat will not completely refreeze in the following winter (Connon et al., 2018). This results in the development of a perennially-thawed (*i.e.,* talik) layer situated between the overlying active layer and the underlying permafrost (Connon et al., 2018). The development of talik not only greatly accelerates permafrost thaw (Connon et al., 2018), but also introduces a year-round subsurface flowpath below plateaus (Devoie et al., 2019). Wildfire has been observed to trigger the development of perennially-thawed taliks, both in the subarctic region of Canada (Gibson et al., 2018) as well as Alaska (Nossov et al., 2013), with implications for hydrological, thermal and geochemical transport.

As ice-rich permafrost thaws, the overlying ground surface subsides. This process inundates and transforms the plateau to a treeless, permafrost-free wetland (Beilman and Robinson, 2003). By transforming a plateau to a wetland, permafrost thaw therefore also transforms the hydrological function of the land cover as an area formerly occupied by a plateau is no longer able to impound adjacent wetlands. Likewise, permafrost thaw can also transform the hydrological function of the adjacent wetlands. In the case of hydrologically-isolated wetlands, the transformation is from one of water storage to one of flow conveyance whereby the thaw of permafrost between wetlands allows water to cascade from one wetland to another in a manner similar to the 'fill-and-spill' principle (Spence and Woo, 2003). This

process of 'wetland capture' (Connon et al., 2014) also increases the hydrological connectivity of the landscape (Haynes et al., 2018). Permafrost thaw can therefore reduce wetland water storage and expand the runoff producing area, and as such is believed to have contributed to the transient and permanent increases in basin discharge observed throughout the southern Taiga Plains (Haynes et al., 2018).

In addition to driving permafrost thaw, fires also affect the flux and storage of water in other ways. By transitioning forests to open environments, wildfires can reduce canopy interception and subsequent sublimation of snow, and thereby increase the snow accumulation on the ground, and the snow water equivalent available for runoff at the end of winter (Pomeroy et al., 2008; Gleason et al., 2013). Charring of the forest floor can increase the heat flux into the ground and the subsurface energy storage (Harden et al., 2006), increasing seasonal thaw depths following wildfire (Koch et al., 2014; Brown et al., 2015), and exacerbating permafrost thaw (Jafarov et al., 2013; Koch et al., 2014). Heating and scorching of the ground surface can produce a hydrophobic layer that can persist for several years, impeding both infiltration and upward moisture migration (Kettridge et al., 2014; Koch et al., 2014). Combustion of the highly-conductive near-surface peat layer effectively brings the deeper, more senescent peat closer to the new (lowered) ground surface (Flannigan et al., 2009; Sherwood et al., 2013), thereby reducing the rate of subsurface drainage and increasing near-surface moisture storage (Thompson and Waddington, 2013; Brown et al., 2015).

Permafrost thaw and other fire-induced changes to peat plateaus have the potential to alter the geochemical environment. Close to the ground surface where the horizontal hydraulic conductivity is uniformly high, water and solutes are conducted rapidly through large, open and connected inter-particle pore spaces (Holden, 2009; Price and Whittington, 2010). However, if this layer is diminished or removed by fire, or if the increased ground heat flux following a fire displaces the saturated layer deeper into the profile, water must flow through smaller peat pore diameters and more tortuous pathways (Rezanezhad et al., 2016; McCarter et al., 2020). This greatly increases the opportunity time for chemical evolution of subsurface water while draining from the plateau. Following a wildfire, the chemistry of the water in the saturated layer of a peat plateau may therefore be more influenced by water-soil interactions. Where permafrost thaw results in talik development, such layers can provide an anoxic environment for redox-type reactions, while enabling change in solute (*i.e.,* nutrients and contaminants) transport throughout the year. Peat plateaus overlying thawing permafrost have been found to release dissolved organic carbon (DOC) and dissolved organic nitrogen (DON) that was previously immobile (Gordon et al., 2016), thereby potentially increasing their export from basins (Schuster et al., 2011). Furthermore, permafrost thaw below peat plateaus is also known to increase methylation of mercury in local areas of recent permafrost thaw (Gordon et al., 2016). However, the biogeochemical impacts following wildfire have yet to be investigated in the peat plateau-wetland complexes of the discontinuous permafrost zone.

This study aims to improve the understanding of how wildfires can alter the flux and storage of water within a peat plateau, and how these hydrological changes in addition to other fire-induced physical changes affect the flux of water and solute from the plateau to downslope ecosystems. This was achieved using a comprehensive series of hydrological, biogeochemical, permafrost and peat physical measurements in an effort to develop a framework for the coupled hydrological, thermal, and biogeochemical response to wildfire in peat plateau-wetland complexes. This multi-faceted approach involving both field and laboratory analyses facilitated the ability to holistically demonstrate the dynamic interplay between the hydrological, thermal and biogeochemical processes and feedbacks triggered by a wildfire event in the discontinuous permafrost landscape, which has not been previously examined in the literature.

2. Study site

Scotty Creek (61°18′ N, 121°18′ W) drains a 152 km^2 peatland-dominated basin underlain by discontinuous permafrost in the southern Taiga Plains ecoregion, 50 km south of Fort Simpson, Northwest Territories (NWT), Canada (Fig. 1a). This region has a dry continental climate with short dry summers and long cold winters, with the typical growing season spanning May to October. For the period 1981–2010, the mean annual air temperature at Fort Simpson was −3.2 °C, and the mean annual total precipitation was 369 mm, of which 145 mm (~39%) fell as snow (Meteorological Services of Canada, 2012). Snowmelt usually commences between late March and mid-April and can last until early May (Hamlin et al., 1998). Scotty Creek drains a continuous organic terrain covered by a mosaic of peat plateaus, collapse scar wetlands and channel fens, with peat depths ranging from 2 to 8 m (McClymont et al., 2013). The peat soils in this basin are classified as histosols, with the permafrost-cored peat plateaus classified as cryosols (IUSS Working Group WRB, 2015). On 18 June 2014, a naturally-ignited wildfire in the headwaters of the Scotty Creek watershed (Fig. 1b) burned a 1.5 ha portion of a 2 ha peat plateau (P1) as well as approximately half of a 5 ha plateau (P2) (Fig. 1c). The fire was extinguished within 24 h. The fire was considered to be of low severity in terms of ground surface damage, with only singeing of the surface peat (Keeley, 2009).

The vegetation of the unburned portion of P2 is dominated by black spruce (*Picea mariana*) trees, and shrubs including Labrador tea (*Rhododendron groenlandicum*), dwarf birch (*Betula glandulosa*) and bog cranberry (*Vaccinium oxycoccos*). The ground cover is comprised mainly of *Sphagnum* moss and *Cladina* lichen species which together produce hummock-hollow type microtopography over the plateau surface, whereby the hummocks rise 0.3 to 0.6 m above the surrounding hollows. As such, the hummock surfaces are relatively dry compared with the intervening hollows (Zoltai and Tarnocai, 1975). The landform types, including peat plateaus, characteristic of the Scotty Creek basin have been extensively studied for nearly three decades (Quinton et al., 2019). There is a high degree of similarity among peat plateaus in terms of black spruce canopy structure, understory vegetation, peat species and hydraulic properties, as well as thermal and permafrost characteristics (Quinton et al., 2019). Therefore, given that this wildfire was not a prescribed burn, it was assumed that the unburned plateaus examined in the present study represent the pre-burn condition of the burned sites.

3. Methods

3.1. Measurement framework: stations, transects and plots

Meteorological stations were installed in each of the burned and unburned portions of P1 in August 2014 (Fig. 1). Both were instrumented to measure and record air temperature (T_a; °C), snow depth (d_s; m) (SR50A acoustic sensor, temperature corrected, Campbell Scientific, Edmonton, AB), wind speed (U_z; m s^{-1}) at 3 m above the ground surface (RM4 standard cup anemometer, Model 05103, Traverse City, MI), and incoming and outgoing shortwave (K_{in}, K_{out}) and longwave (L_{in}, L_{out}) radiation at 3 m above the ground surface (CNR4, Kipp and Zonen, Delft, Netherlands; see Table S1). All measurements were made at one-minute intervals and averaged and recorded every 30 min (Table S1) using a Campbell Scientific data logger (Logan, UT). Precipitation (rain and snow) was measured and recorded using a Pluvio (OTT Hydromet, Loveland, CO) weighing gauge on the north side of Goose Lake, approximately 2 km from the study sites.

In March 2016, two transects and six plots were established at P2 (Fig. 1c). The transects were each ~200 m long, spanned the burned and unburned portions of P2, and used for measurements of snow depth and density, ground thaw, and soil moisture. Each plot was ~100 m^2, three of which (B1–B3) were located in the burned and

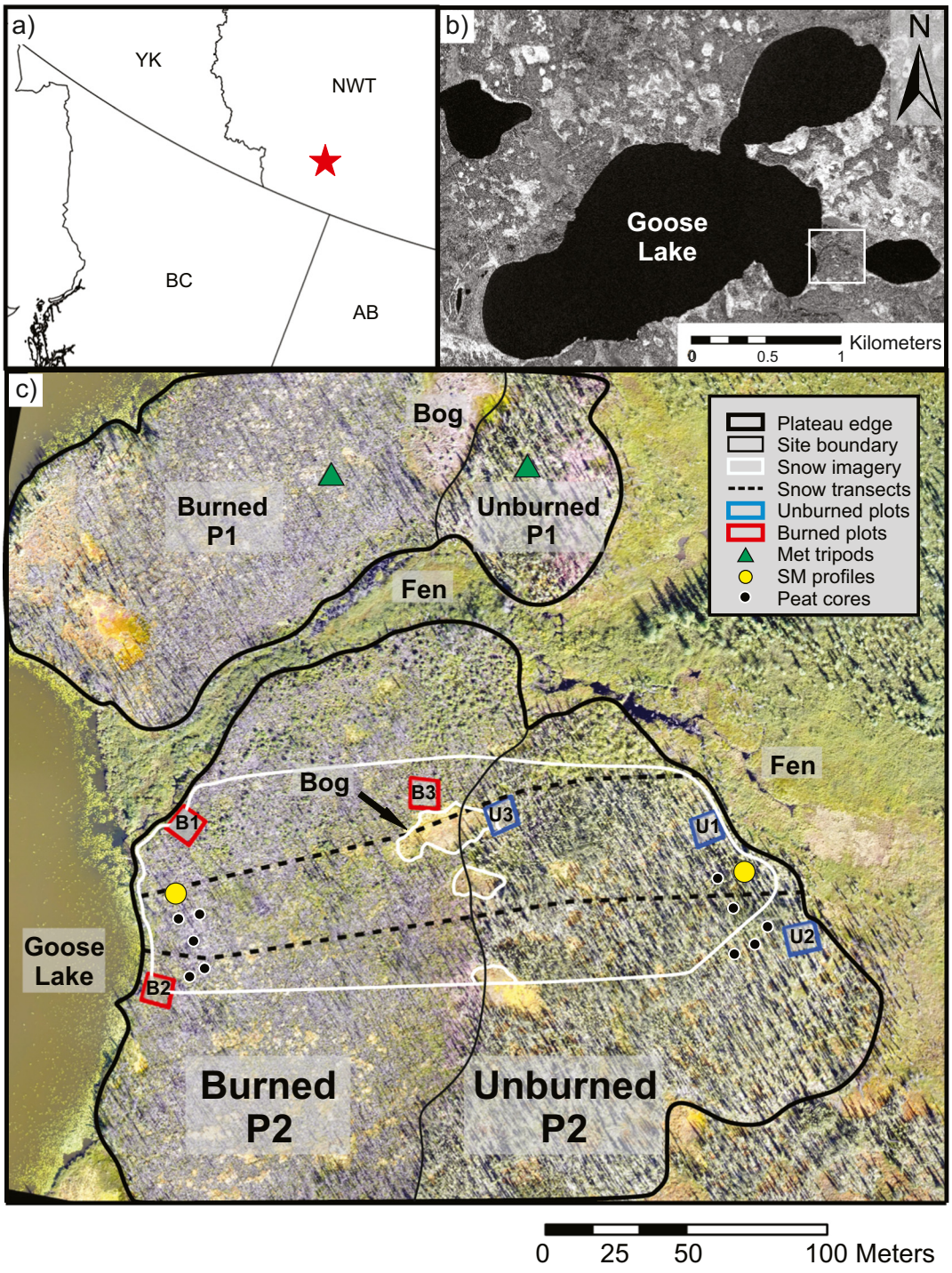

Fig. 1. (a) Location of Scotty Creek, Northwest Territories, Canada. (b) Study area that includes the partially burned peat plateaus and Goose Lake. (c) Aerial imagery of the partially burned plateaus (P1, P2), locations of study sites (burned, unburned), study plots (B1–B3, U1–U3), snow survey transects, UAV snow imagery boundary (see Fig. 3), locations of soil moisture (SM) probes, meteorological stations, and peat cores.

three in the unburned (U1–U3). Given that the objective of this study is to examine the effects of wildfire on the flux and storage of water and solute from peat plateaus to downslope ecosystems, the locations of the plots were selected based on likely flowpaths. On the burned portion of P2, plots B1 and B2 were chosen to represent the dominant flowpaths from the plateau to adjacent fen and lake (Fig. 1c). Similarly, plots U1 and U2 on the unburned portion of plateau P2 were delineated to capture the flowpaths along the hydraulic gradient from the plateau to the adjacent channel fen (Fig. 1c). The locations of B3 and U3 were selected to capture the potential transport to a developing collapse scar wetland, which is internally drained (Fig. 1c). Plots were used for detailed measurements of ground thaw, water table depth, and collection of pore water samples for solute analyses (Table S1).

3.2. Snowpack measurements

Snow depth and density were measured at 5 m and 25 m intervals, respectively, along both transects at the end of winter in 2016 using a

Prairie Snow Sampler (Geo Scientific, Vancouver, BC, Canada) and electronic scale (Light Duty Crane Scale; BC Scale, Langley, BC, Canada). These measurements began on 27 March 2016 and were repeated every second week until the final measurements on 25 April 2016 (Table S1). The snow water equivalent (SWE; mm) was computed from the snow depth at each point and the transect-average snow density. An unmanned aerial vehicle (UAV; DJI Phantom 2, Shenzhen, China) with a 14 Megapixel camera was flown daily over P2 (Fig. 1c) at a height of 30 m above the ground surface to monitor the areal depletion of snow (Table S1). Images were processed in Pix4Dmapper (Lausanne, Switzerland), and converted to binary format using ArcMap (ESRI, Redlands, CA).

3.3. Ground thaw

As the measurement points along the two transects used for snow surveys became snow-free, they were used to measure depth to the frost table using a 150 cm graduated steel probe (Table S1). Once plots were established, frost table depth was also measured on a finer scale within each plot using a grid with 0.5 m between measurement points. The absolute elevation of the ground surface at each grid point was measured using a digital GPS (Viva GS10, Leica Geosystems AG, Switzerland, RTK $\pm$ 0.02 m accuracy). Gridded measurements of frost table depth across all six plots took up to five days to complete and were made in the following periods: 22 to 24 May 2016, 30 June to 3 July 2016 and 25 August to 1 September 2016. Digital elevation models (DEMs) of the ground surface and frost table were generated for each plot using the kriging method (Surfer, Golden Software, Golden, CO) to illustrate seasonal frost table depth progression, and to identify frost table depressions and preferential subsurface flow paths. The topographic variability of the ground and frost table surfaces were characterised by the vector ruggedness measure (VRM) following the method of Sappington et al. (2007). The volume of depressions in the frost table topography (depression storage, S_d) was computed for each plot using Whitebox GAT (Lindsay, 2016).

3.4. Water table and soil moisture

Water table elevation was measured and recorded every 30 min at two 5-cm inner diameter wells in each plot using a HOBO pressure transducer (Bourne, MA), corrected for atmospheric pressure using measurements from a thermally-buffered barometer (HOBO U20; see Table S1). Soil moisture was measured and recorded every 30 min at one instrumented profile located in both the burned and unburned portions of the plateau P2 (see Fig. 1c for the locations of the soil moisture (SM) profiles) with 5TM sensors (Decagon, Pullman, WA; see Table S1) at 5, 10, 15, 20 and 30 cm below ground surface. Because these sensors were not calibrated *in situ*, these data were used only to indicate relative differences between the sites and over time.

3.5. Chemistry of snowmelt and pore water

Snow pits were excavated at each of the burned and unburned plots on 28 March 2016 using Teflon-coated shovels. In each pit, snow was sampled from the major snow layers using a 200 cm^3 polyethylene scoop that had been immersed and rinsed with deionized water. The samples were then stored in pre-rinsed polyethylene, re-sealable bags, and allowed to melt at 20 °C before processing for analysis. Following snowmelt, peat pore water was sampled from the saturated layer at each plot from two holes (~10 cm diameter) excavated down to the frost table at each of the six plots using a polyethylene trowel rinsed in 18.2 MΩ Milli-Q water. These holes were re-sampled throughout the study period, progressively deepening each hole as the frost table lowered with thaw and were capped with the extracted peat in between sampling events. Pore water sampling began on 7 May 2016 and was repeated weekly until 6 June 2016, with additional samples collected from each well on 3 July 2016 (Table S1). Samples were obtained using a pre-washed, sample-rinsed 250 mL bottle (Thermo Fisher Nalgene) lowered below the water table and filled.

With the exception of samples taken for the analysis of dissolved total mercury (THg) and methylmercury (MeHg), all samples were sequence-filtered in the field, first through 0.7 μm glass fibre filters (GF/F), and then through 0.45 μm cellulose acetate filters (Sartorius). The samples for cations were preserved with 18% trace metal grade nitric acid (HNO_3) to a final pH < 2. Samples for analysis of dissolved THg and MeHg were collected using the "clean hands-dirty hands" technique and filtered using pre-cleaned (with 1% trace metal grade hydrochloric acid (HCl)), 18.2 MΩ Milli-Q water rinsed disposable filter packs (Fisher 126–0045 CN Filter Unit, 250 mL), and preserved with ultra-trace metal grade HCl. All pore water samples were kept cool and dark until shipment to the Canadian Association for Laboratory Accreditation-certified Biogeochemical Analytical Service Laboratory (BASL) at the University of Alberta (Edmonton, Alberta, Canada) for analysis. Samples are referred to as snowpack (28 March 2016), freshet (7 May 2016), early-season (16 May-6 June 2016), and mid-season (3 July 2016).

Dissolved organic carbon (DOC) was analyzed using a Shimadzu TOC-5000A analyzer, following methods described in Littlefair and Tank (2018). Total dissolved nitrogen (TDN) and total dissolved phosphorous (TDP) were analyzed using a Lachat QuickChem QC8500 FIA Automated Ion Analyzer (Lachat, Loveland, Colorado, US) (American Public Health Association, 2017, Methods 4500-P and 4500-N). Cations (Na^+, K^+, Ca^{2+}, Mg^{2+}, Al^{3+} and dissolved Fe [dFe]) were analyzed using a Thermo Scientific ICAP-6300 Inductively Coupled Argon Plasma - Optical Emission Spectrometer (US EPA Method 200.7, 1994) and anions (Cl^-, SO_4^{2-}) using a Thermo Scientific Dionex DX-600 Ion Chromatograph (Thermo Fisher, Waltham, Massachusetts, US) (US EPA Method 300.1, 1997). Dissolved THg and MeHg were analyzed using Tekran 2600 Total Mercury Analyzer (Toronto, Ontario, CA; US EPA Method 1631, 2002) and Tekran 2700 Methyl Mercury Analyzer (US EPA Method 1630, 1998), respectively. Details on the method detection limit (MDL) and limit of quantification (LOQ) for all analyzed constituents are provided in Table S2.

3.6. Peat physical and hydraulic properties

At both the unburned and burned sites, five vertical peat cores, each 4 cm in diameter and collected from 0 to 20 cm depth, were analyzed for physical and hydraulic properties (Fig. 1c; Table S1). These cores were collected to represent the natural variation in ground cover present in both the unburned and burned plateau sites. At each site, two cores were taken from moss-covered and two from lichen-covered ground surfaces (in the burned site, moss and lichen were charred, but still recognizable). An additional sample was taken from a burned depression at the burned site, and from un-vegetated ground at the unburned site. Following the methods of Sherwood et al. (2013), each core was divided into ten 2 cm sub-cores, each representing a 2 cm depth range of the overall core. The sub-cores, referred to by their mid-point (*e.g.,* 4–6 cm depth range referred to as 5 cm), were used to create detailed depth profiles of physical and hydraulic properties. Samples were fully submerged in 18.2 MΩ MilliQ water for one week prior to testing to obtain a saturated volume. Following the completion of all tests, which were performed sequentially on subsets of depths from all 10 collected peat cores (with the number of sub-cores for each test specified below), sub-cores were oven dried at 80 °C for 48 h to obtain dry weight (w_{dry}; g), bulk density, (ρ_b; g cm^{-3}; $n = 59$ sub-cores), total porosity (ϕ_T; cm^3 cm^{-3}; n = 59 sub-cores), and effective porosity (ϕ_{EFF}, cm^3 cm^{-3}; n = 59 sub-cores), sometimes referred to as field capacity and defined here as the relative pore volume drained at 100 mbar of pore pressure (see below).

The vertical saturated hydraulic conductivity (K_{sat}; m d^{-1}) was measured for each sub-core ($n = 67$ in total) using a modified constant head

method. Mini-permeameters were constructed using the sub-core rings as the permeameter walls, extended vertically by 2 cm using rigid tape, and constrained on the bottom by muslin cloth. To minimize edge effects, each sub-core was frozen to maintain core integrity, tightly wrapped with heat-sealed Parafilm, and placed back into the plastic ring with extra Parafilm encasing the ring (McCarter et al., 2019). The mini-permeameter was supported by a funnel and ring stand while 1 L of deionized water was run through the thawed sample, maintaining a constant head. K_{sat} was calculated using Darcy's Law, following the method of Huang et al. (1995).

Soil water retention was measured using a pressure plate (Soilmoisture Equipment Corp., Goleta, CA) with volumetric soil moisture contents (Θ) measured at 20, 40, 80, 100, 500 and 1000 mbar. The sub-cores ($n = 27$ in total) were submerged in 18.2 MΩ MilliQ water for one week, then fully saturated, subjected to incremental increases of pore water pressure (ψ) until pore water drainage ceased and hydrostatic equilibrium was achieved. The air entry pressure at each pressure increment corresponded to the maximum opening diameter of pores emptied. Water retention curves were then constructed for each sub-core where Θ was calculated using the measured sample volume for each ψ increment to account for shrinkage upon drying. Pore diameter (d_p; mm) was calculated (Hayward and Clymo, 1982; Nimmo, 2004) assuming a contact angle equal to 40° due to the moderate hydrophobicity of both burned and unburned organic soils (Kettridge et al., 2014).

Dual-porosity characteristics of the sub-cores collected from the burned and unburned moss-covered ground surfaces were examined near the surface (5 cm; $n = 4$ in total) and in deeper peat (15 cm; n = 4 in total) using flow-through experiments to compare fire-induced changes to the dominant water and solute transport mechanisms. The flow-through experiments were conducted at the Ecohydrology Research Group laboratory at the University of Waterloo (Waterloo, Ontario, Canada) using a non-reactive Cl^- tracer following the methods of Kleimeier et al. (2017) and McCarter et al. (2019). The flow through reactor (FTR) contained the slice of heat-sealed parafilm wrapped sub-core placed in a Plexiglas ring of 2 cm length and 4.2 cm inside diameter, on which a nitrocellulose polypropylene membrane filter (0.2 μm pore size, 50 mm diameter, Pall Life Sciences) and a fibreglass filter (1 μm pore size, 47 mm diameter, Pall Life Sciences) backing was placed. The FTR were sealed with PVC plates and O-rings and tightened using stainless steel screws. To purge residual ions and entrapped air, samples were saturated from the bottom and flushed with 18.2 MΩ Milli-Q water for one week while effluent electrical conductivity (EC) was monitored (Thermo Fisher Orion 9617BNWP Chloride Selective Electrode, Waltham, MA) to determine when ion flushing was complete. Once fully flushed, a NaCl solution with initial Cl^- concentration (C_o) of 120 mg L^{-1} was introduced at a constant flowrate of 1 mL h^{-1} using a peristaltic pump (Gilson MINIPULS 3). Effluent volume was measured every 3–4 h, then filtered through a 0.2 μm pore size polysulfone filter and analyzed for effluent Cl^- concentrations (C; mg L^{-1}) by Ion Chromatography (Dionex ICS-5000; ± 3.0% error and ± 1.6% precision). A zero dead-volume blank correction using an extra flow-through reactor (Rajendran et al., 2008) was performed.

A mobile-immobile non-equilibrium flow model (van Genuchten and Wagenet, 1989) was then fit to the observed effluent concentrations in CXTFIT (Toride et al., 1995). The mobile pore water velocity, dispersivity, mobile pore fraction, and mass transfer coefficient were estimated using a nonlinear least-squares parameter optimization. Because Cl^- can be considered a non-reactive solute at low concentrations (McCarter et al., 2019), the solute retardation factor was set to 1. Breakthrough curves were plotted using relative Cl^- concentration (C/C_o) *versus* number of pore volumes of solute passed through the sample. One pore volume, or total porosity, was determined as the volume of water lost from each saturated sample when oven dried at 60 °C until constant weight. For a more detailed explanation of the model parameters for a dual-porosity medium, please see Rezanezhad et al. (2012), Kleimeier et al. (2017) and McCarter et al. (2019).

3.7. Statistical analyses

Significant differences of various physical and chemical measurements between burned and unburned sites were evaluated using mixed effect models using the "*lmer*" function in the "*emmeans*" package (Lenth, 2020) in R Statistical Software (R Development Core Team, 2018). The resultant estimated marginal means were then compared using a post-hoc Tukey test (Lenth, 2020).

For frost table depth (FTD, cm), the ln of the measured frost table depth was used as the dependent variable following

$$ln\,FTD = site * month + (1|\,plot)$$

where, *site* is either the burned or unburned site, *month* is the month of the measurement, and *plot* is the specific measurement plot. Measurement depths exceeding 80 cm were assumed to include a talik (Connon et al., 2018) and excluded from statistical analyses.

Differences in pore water chemistry for each measured solute were determined from

$$ln\,conc = site * season + (1|\,well)$$

where, *conc* is the measured concentration (mass volume^{-1}) of a given solute, *site* is either the burned or unburned site, *season* is either snowpack (representing the chemical concentration of the snowpack prior to the onset of melt), snowmelt (early May 2016), early season (mid-May–early June 2016) or mid-season (July 2016), and *well* is the specific well ID associated with the measured concentration. For snowmelt and pore water chemistry data, concentrations below the MDL (less than 1% of all samples analyzed) were estimated to be one-half of MDL (Mueller and Spahr, 2005).

Lastly, the differences in hydrophysical properties were assessed by,

$$hp = site * depth + (1|\,coreID)$$

where, *hp* is the specific hydrophysical property, *site* is either the burned or unburned site, *depth* is the specific depth of the sample, and *coreID* is the core number. The ln of bulk density and porosity, and $\log_{10}$ of K_{sat} were taken for input into the mixed effect model.

4. Results

The burned areas on P1 and P2 sustained total combustion of the tree canopy, but the fire did not yield significant damage to the ground surface peat beyond singeing. This wildfire event, therefore, likely involved fire spread predominantly through the tree canopy, with only the charred trunks of the trees remaining on the landscape. Given that this wildfire was naturally-ignited rather than a prescribed burn, the amount of organic matter lost from the peat could not be quantified. Soil combustion was most pronounced at the base of charred trees where burn-depressions had formed, while peat soil surfaces away from trees were more lightly burned, with moss and lichen fragments still identifiable. This wildfire resulted in minimal ground surface damage, with only singeing of the surface peat. Despite the surface peat singeing, several metres of intact peat remained following the fire event.

4.1. Meteorological data

While the average daily wind speed (U_z) was consistently higher in the burned plateau throughout the snow-covered (1 Mar–30 April 2016) and snow-free (1 May–26 August 2016) periods of this study (Fig. 2), the average daily air temperature (T_a) was indistinguishable between sites (Fig. 2). During the snow-covered period, the burned site received greater mean daily incoming shortwave radiation (K_{in}) and, due to higher snowpack albedo (α) produced greater mean outgoing shortwave radiation (K_{out}; Fig. 2). During the snow-free period, the burned

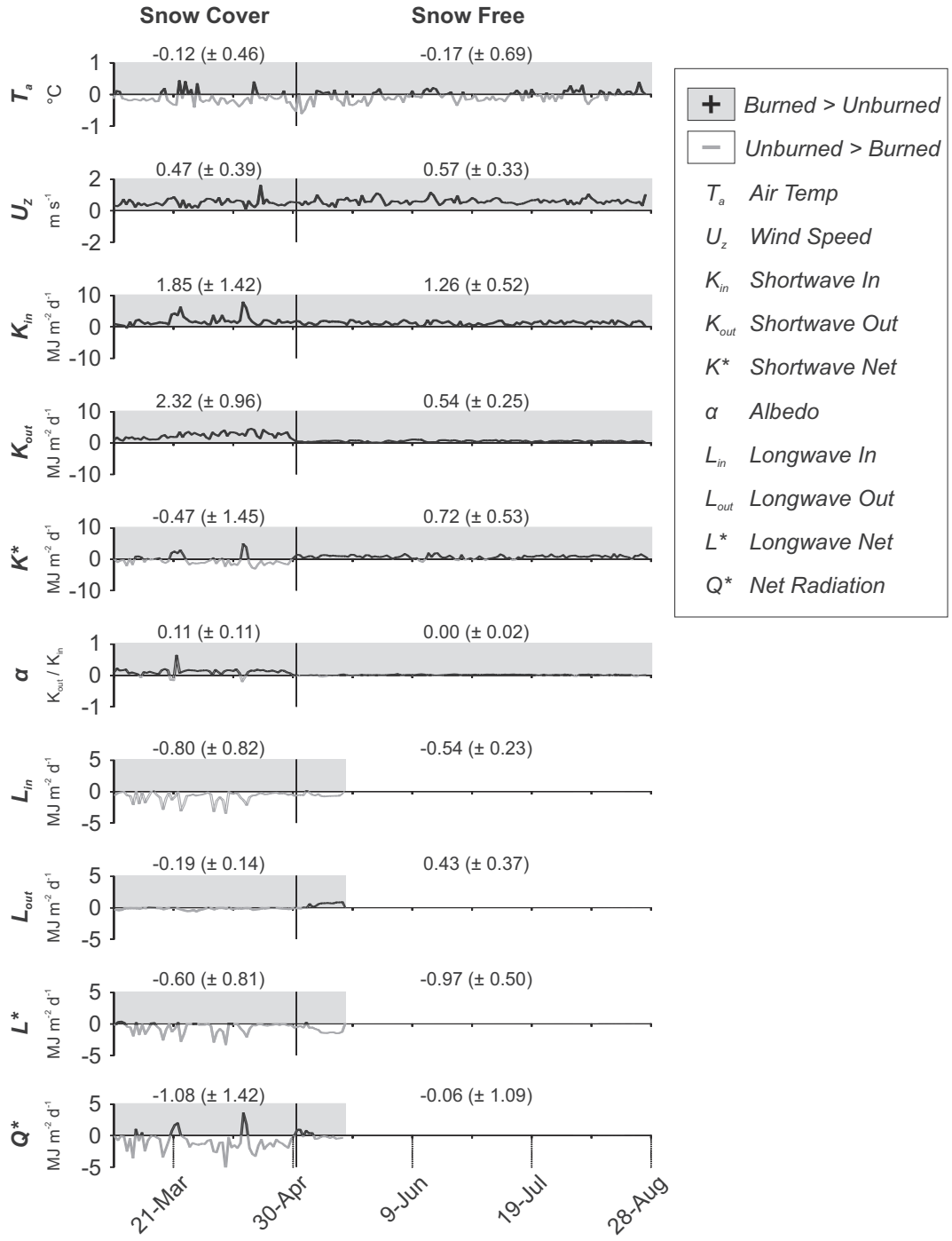

Fig. 2. Difference of daily mean (±1SD) of meteorological parameters between those measured at the burned and unburned sites on peat plateau P1 during the snow cover (1 March–30 April 2016) and snow free (1 May–28 August 2016) periods. Positive values (black line, gray shading) indicate higher daily averages in the burned, and negative values (gray line, no shading) indicate higher daily averages in the unburned. The extent of the gray shading indicates the length of data collection. Note the snow free period for incoming and outgoing longwave radiation (L_{in} and L_{out}), and therefore net radiation (Q*), spanned only 1 May to 16 May 2016 due to an equipment malfunction.

site continued to receive a greater mean K_{in} and produce a moderately higher K_{out}, with the result being a higher net shortwave (K^*) flux (Fig. 2). Both incoming longwave (L_{in}) and outgoing longwave radiation (L_{out}) were marginally greater in the unburned site during the snow-covered period, however, once the ground surface became snow-free, L_{in} remained slightly higher in the unburned while L_{out} emitted from the burned site was greater (Fig. 2).

On 1 December 2015, the mean snowpack depth measured at the burned site meteorological station on P1 was 61% of the depth of the unburned snowpack (SR50A; unburned = 45 cm, burned = 27 cm; Fig. 3a). This depth difference diminished over the winter so that by the time snowmelt commenced on 27 March 2016, the snowpack depths at the burned and unburned sites were virtually the same (unburned = 70 cm, burned = 69 cm). Although the burned site snowpack was comparatively shallower, snow surveys showed that it was approximately 10% denser (Fig. 3c) between 27 March and 22 April 2016 and contained 5–6% greater SWE than the snowpack at the unburned site (Fig. 3d). However, snowpack depletion was more rapid at the burned

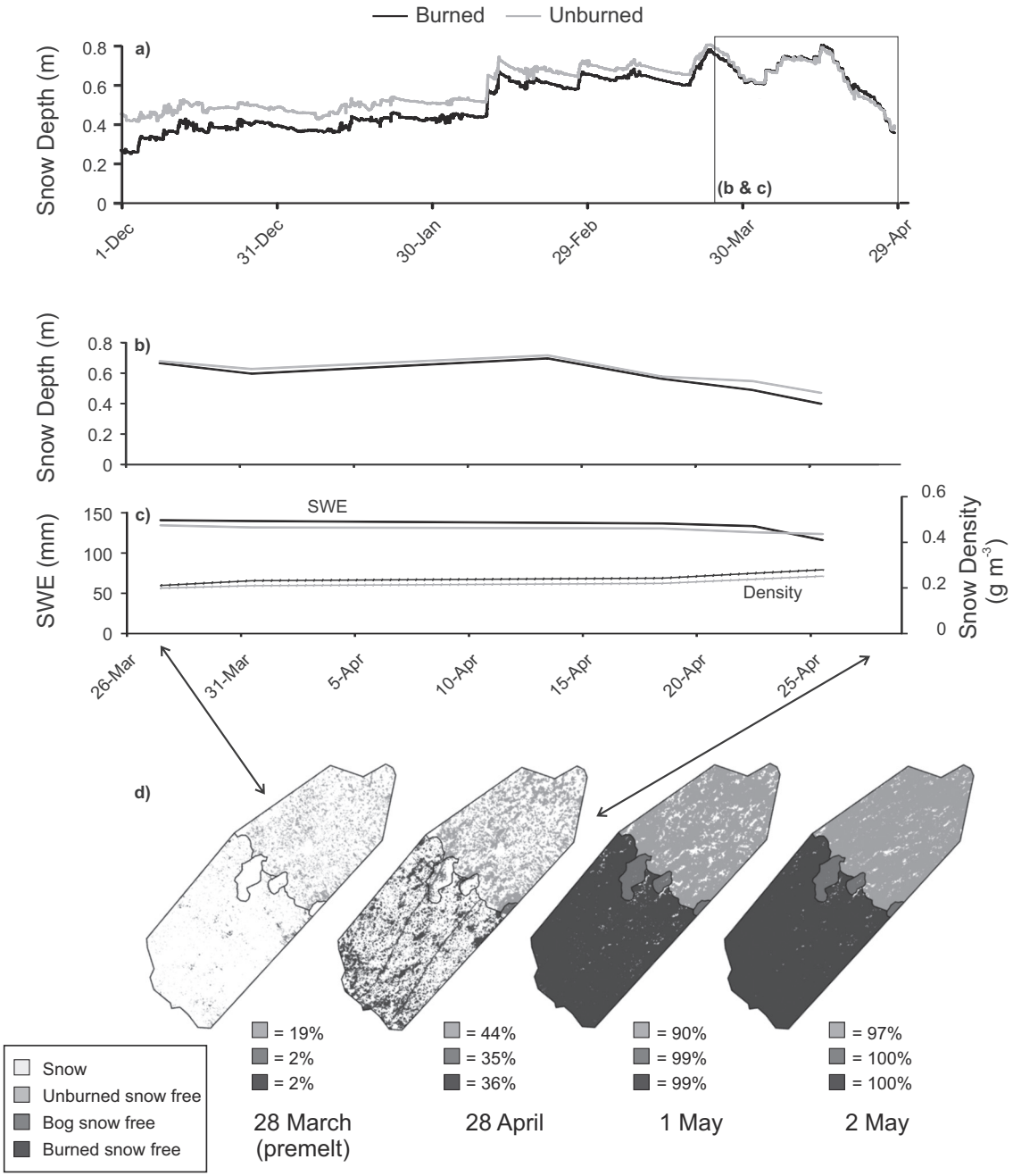

Fig. 3. Snow accumulation and ablation including (a) differences of over winter (1 December 2015–28 April 2016) snow depth measured from SR50A acoustic sensors at peat plateau P1, (b) mean snow depth, (c) mean snowpack density and snow water equivalent (SWE) measured along transects T1 and T2 on peat plateau P2 (see Fig. 1), and (d) percent snow-free area of P2 showing pre-melt vegetation exposure (28 March 2016) and aerial snowpack ablation (28 April–2 May 2016).

site as snowmelt progressed, resulting in a 15% shallower snowpack in the burned area (Fig. 3b) on the final day of snowpack measurement (25 April 2016) and 6% less SWE compared to the unburned site. Furthermore, areal depletion of the snowpack (Fig. 3d) was more rapid at the burned site and as a result, the burned area became snow-free on 2 May 2016, three days before the unburned.

4.2. Ground thaw and soil moisture

The unburned and burned sites had contrasting ($p = 0.09$, Table S3) ground thaw rates and patterns (Fig. 4). While the mean difference in frost table depth (d_{FT}) between sites in May 2016 was not significantly different ($p = 0.995$, Table S3) between the burned (20.3 ± 1.0 cm, estimated marginal mean ± standard error) and unburned (20.9 ± 1.0 cm) sites, by June 2016 the burned site had significantly deeper d_{FT} ($p = 0.06$, Table S3, Fig. 4). By August 2016, there was no significant difference in d_{FT} between sites ($p = 0.51$, Table S3, Fig. 4). The proportion of d_{FT} observations exceeding 80 cm (the threshold for talik determination) was greater in the unburned site, so that by the end of August 2016, 28% of d_{FT} observations exceeded 80 cm in the unburned site, compared to 12% in the burned site. Although the ground surface at the burned site (VRM = 0.0015) was marginally more rugged than at the unburned (VRM = 0.0013; Fig. 5), the differences in frost table ruggedness between the burned and unburned sites were more prominent. At the end of May 2016, the topography of the frost table below the burned site had a slightly higher VRM (0.0017) than the unburned

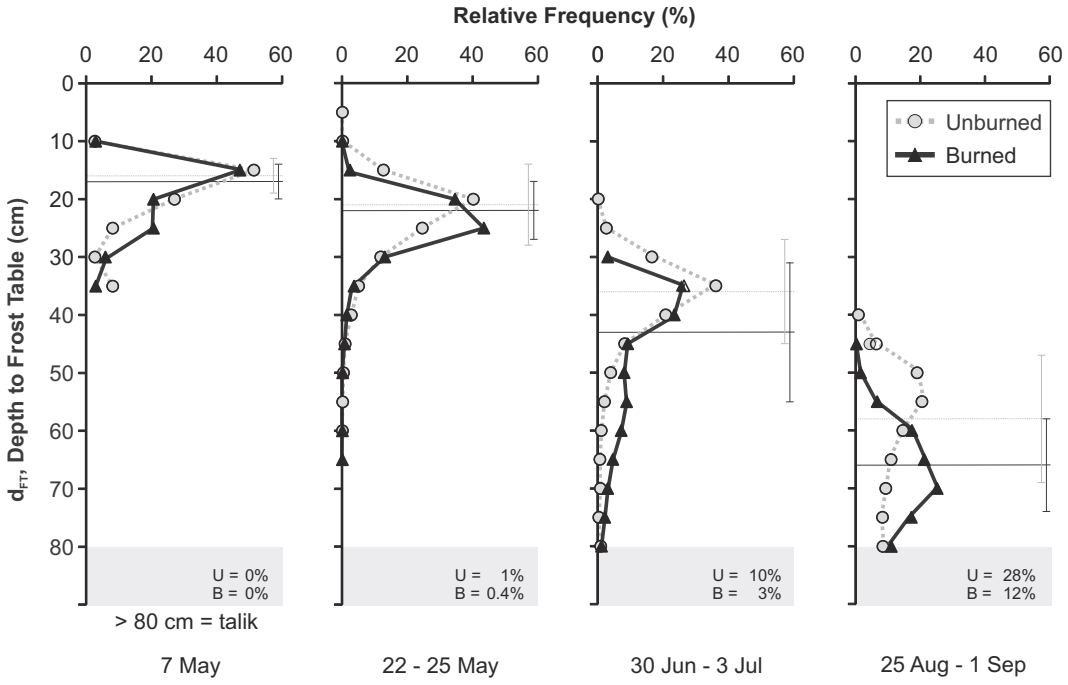

Fig. 4. Relative frequency (%) of depth to frost table (d_{FT}) measured over the thaw season representing aggregated unburned (U1–U3) and burned (B1–B3) study plots. Where $d_{FT} > 80$ cm, probe insertion into talik was assumed; percent of total measurements are reported (shaded gray) and were excluded from statistical analysis.

(VRM = 0.0009), which was coupled with a 57% lower depression storage capacity (S_d; Fig. 5). Ground thaw above the frost table over the subsequent month reversed these conditions so that by the end of June 2016, the burned site displayed a less rugged FT (VRM = 0.0035 for the burned site as compared to 0.0046 for the unburned site) with 29% greater S_d. The DEMs and linear cross-sections parallel to the slope direction (Fig. 5) demonstrate the co-development of water storage depressions and preferential flowpaths both along the ground surface and the frost table as the thaw season progressed at each site (Fig. 5).

The burned and unburned sites also had contrasting *in situ* soil moisture (Θ) (Fig. 6). The burned site was relatively dry ($\Theta = 0.09 \pm 0.01$; mean $\pm$ 1 standard deviation (SD)) at 5 cm depth compared with the unburned site ($\Theta = 0.15 \pm 0.03$). Both sites had a moderately dry layer (mean Θ of approximately 0.2 to 0.3), which was slightly thicker at the unburned site (10 to 30 cm depth) than at the burned site (10 to 20 cm depth). At 30 cm, the burned site was on average wetter ($\Theta = 0.37 \pm 0.06$) than the unburned ($\Theta = 0.17 \pm 0.04$). Thus, in comparison with the unburned site, the peat profile at the burned site can be described as consistently drier in the upper (0 to 5 cm depth) part of the profile but consistently wetter deeper within the profile (20 to 30 cm).

Additionally, the burned and unburned sites exhibited contrasting responses to precipitation, illustrated by the response to a 12 mm event of 10 h duration on 16 June 2016 (Event A; Fig. 6 a and b). At the unburned site, this event generated a modest increase in soil moisture of approximately 0.05 at all measurement points throughout the 30 cm peat profile, followed by a congruent return to pre-event Θ. In contrast, the burned site profile responded with larger, more abrupt increases in Θ at all depths below 5 cm, with the largest rise (from 0.45 to 0.56) occurring at the greatest measured depth (30 cm).

The height of water table rise generated by Event A was of similar magnitude at the two sites; 3 cm at the unburned site and 4 cm at the burned site (Fig. 6 c and d). The water table rise briefly interrupted a general water table recession and general thinning of the saturated layer at the unburned site (*i.e.,* layer between the water table and frost table). In contrast, Event A contributed to a sustained rise in the water table at the burned site (Fig. 6d), resulting in a general thickening of the saturated layer as the study period progressed.

4.3. Water chemistry

Snowpack samples (28 March 2016) contained negligible concentrations of all measured chemical constituents (Fig. 7) and were not significantly different (Table S4) between the burned and unburned sites. Snowpack concentrations of MeHg, Al, Mg^{2+} and dFe were at or below the MDL, while concentrations of THg, TDP, Cl^-, SO_4^{2-} and K^+ were at or below the LOQ (see also Table S2). While concentrations of remaining constituents were slightly above the LOQ, they were also quite low relative to mean pore water concentrations, which were 26- (TDN), 101- (DOC), 93- (Na^+) and 122-fold (Ca^{2+}) that of mean snowpack concentrations. Following snowmelt, both burned and unburned sites in general exhibited a similar temporal pattern of pore water solute concentrations, with an increase in concentrations during the freshet (7 May 2016), followed by a solute concentration peak in the early season (16 May - 6 June 2016), and variable solute concentrations in the mid-season (3 July 2016). However, pore water sampled from the burned sites tended to have greater mean solute concentrations than those in the unburned (Fig. 7, Table S4). Differences in solute concentrations between sites were greatest immediately following snowmelt and decreased with time over the snow-free season.

These general trends were pronounced for some, but not all, pore water chemical constituents. Specifically, mean pore water concentrations of ions (including Ca^{2+}, Mg^{2+}, K^+, Al^{3+}, dFe, Cl^-, SO_4^{2-}, but not Na^+), as well as the SO_4^{2-}:Cl^- ratio, were generally higher in the burned site (Fig. 7, Table S4). For example, mean Ca^{2+} concentrations were 6.8 $\pm$ 1.1 mg L^{-1} (mean $\pm$ 1 SD) greater in the burned during the early snow-free period (7 May-6 June 2016) but this difference decreased with time and became insignificant by 3 July 2016. This temporal pattern was mimicked by all ion species (except Na^+, and only weakly by Cl^-), with concentrations either significantly or marginally greater at the burned sites (Fig. 7, Table S4). Pore water dissolved nutrients (TDN, TDP), organic carbon (DOC), dissolved total mercury (THg) and methylmercury (MeHg) concentrations, and the percent of THg that

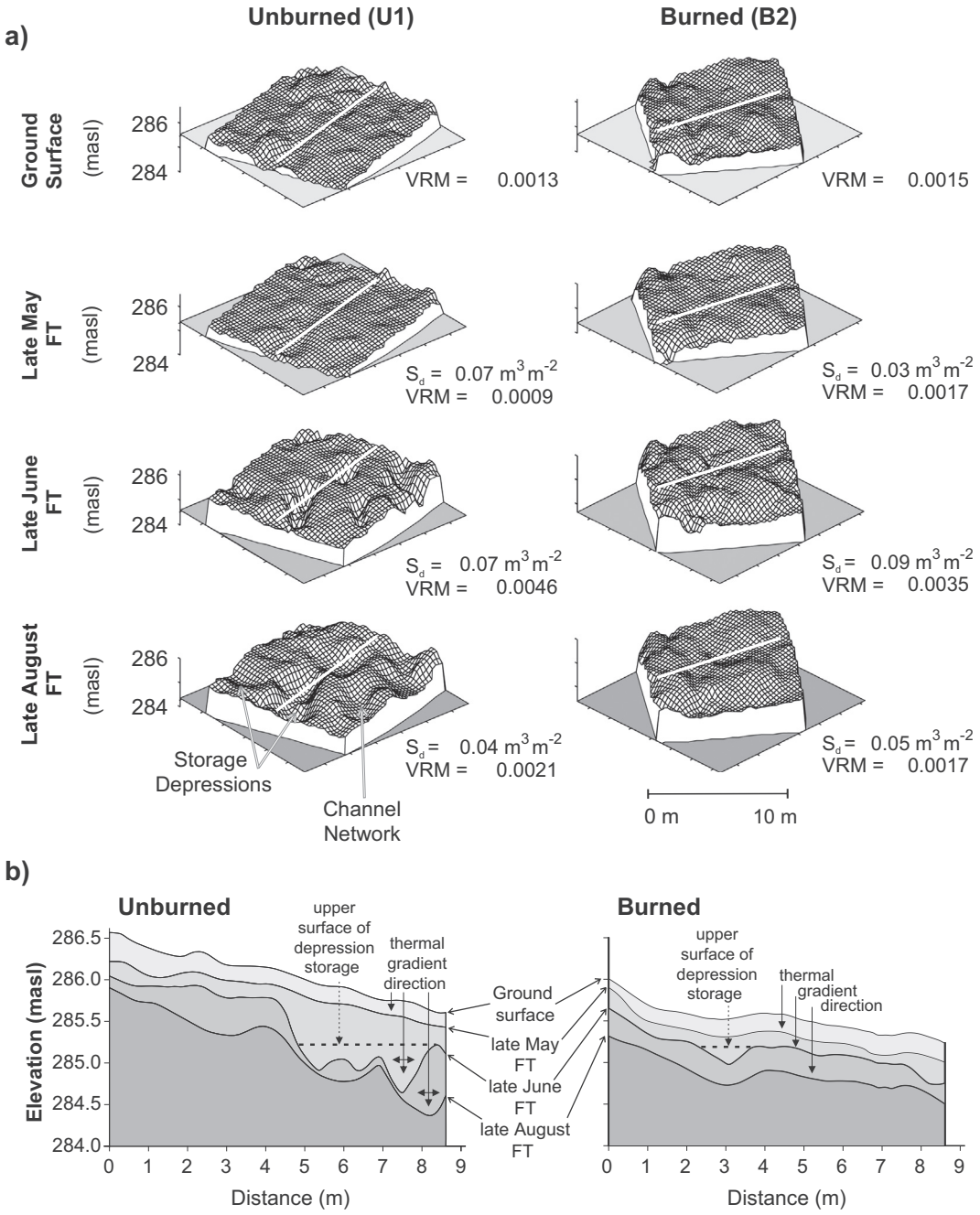

Fig. 5. a) Digital elevation models (DEMs) of gridded plots (U1, B2) showing topography (meters above sea level; masl) of ground surface (GS) and frost table (FT) as thaw progressed. Depression storage (S_d; $m^3\ m^{-2}$) and the unitless FT vector ruggedness measure (VRM; unitless) along the preferential flowpaths were calculated for aggregated plots within each site (U1–3, B1–3). Planes intersect the z-axes at the lowest measured GS point (top row), and deepest $d_{FT} \leq 80$ cm (bottom three rows). White lines along preferential runoff flowpaths indicate the location of cross-sections illustrated in b) Cross-sections of DEMs for the unburned and burned sites showing seasonal frost table (FT) evolution relative to the ground surface, depression storage, and the direction of the thermal gradient.

was in the form of MeHg (%MeHg) were also typically higher at the burned (Fig. 7, Table S4). Methylmercury concentrations were significantly higher at the burned site ($p = 0.002$, Table S4) driven by significant increases during the freshet ($p = 0.09$) and mid-season ($p = 0.006$), while THg was only significantly higher during the mid-season (Table S4). Mean pore water concentrations of DOC and TDP were 33.8 ± 5.3 mg L^{-1} ($p < 0.001$) and 1.5 ± 0.5 mg L^{-1} ($p = 0.07$), respectively, greater at the burned site throughout the sampling season. Total dissolved nitrogen was 2.0 ± 0.5 mg L^{-1} higher in the burned site through early-season ($p < 0.003$), but not significantly different from the unburned site during the mid-season. However, TDN was significantly greater overall at the burned site relative to the unburned site ($p = 0.001$).

4.4. Peat physical and hydraulic properties

Average bulk density (ρ_b) was significantly greater in burned site cores ($p = 0.02$, Table S5), driven by increases in ρ_b at all depths but no single depth was significantly different between sites (Fig. 8a, Table S5). However, there was a clear observable increase in ρ_b with depth from 0.06 to 0.10 g cm^{-3} between 3 and 17 cm in the unburned site and from 0.10 to 0.16 g cm^{-3} in the burned site (Fig. 8a). At both

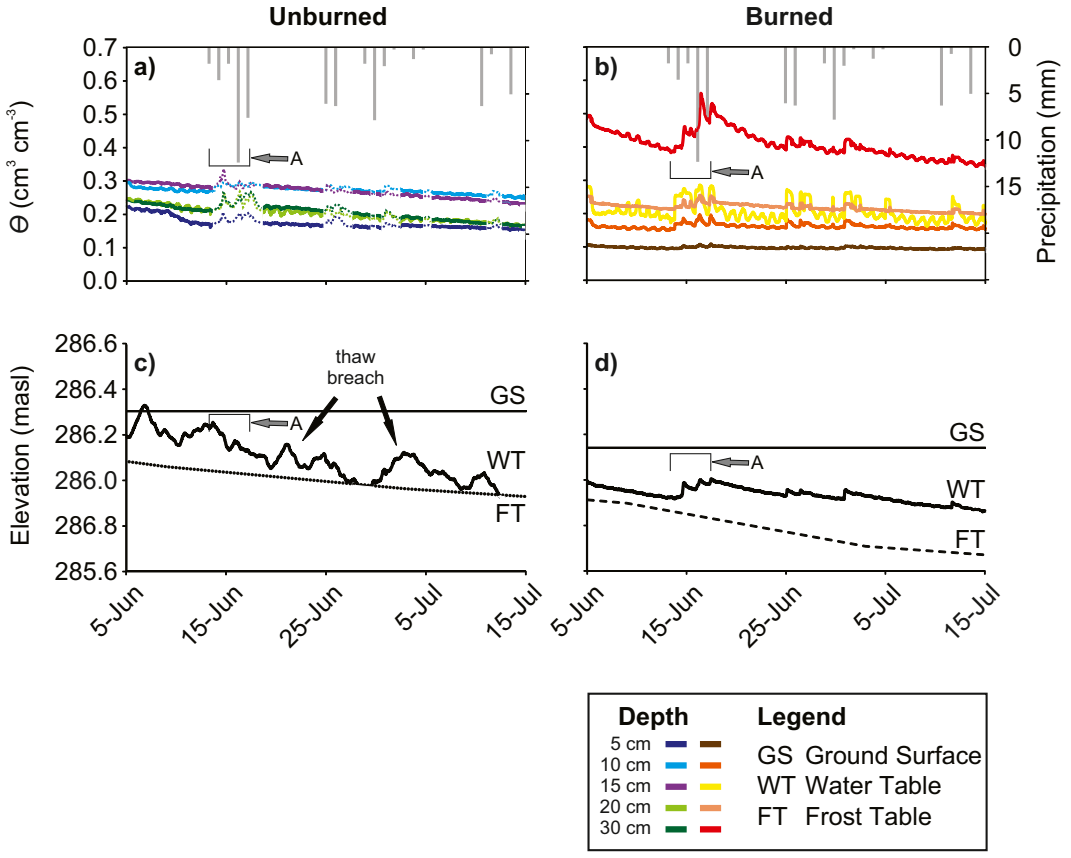

Fig. 6. Soil moisture (Θ) profiles between 0 and 30 cm below ground surface in the unburned (a) and burned (b) sites, and water table (WT) responses to precipitation, relative to the ground surface (GS) and frost table (FT) as thaw progresses in the unburned (c) and burned (d) sites. Precipitation Event A occurred on 16 June 2016. Water table rise in the unburned site without precipitation is indicative of water released from storage following thaw breach of a frost table depression wall (c). Note dashed lines in panel (a) indicate estimated Θ values due to equipment malfunction.

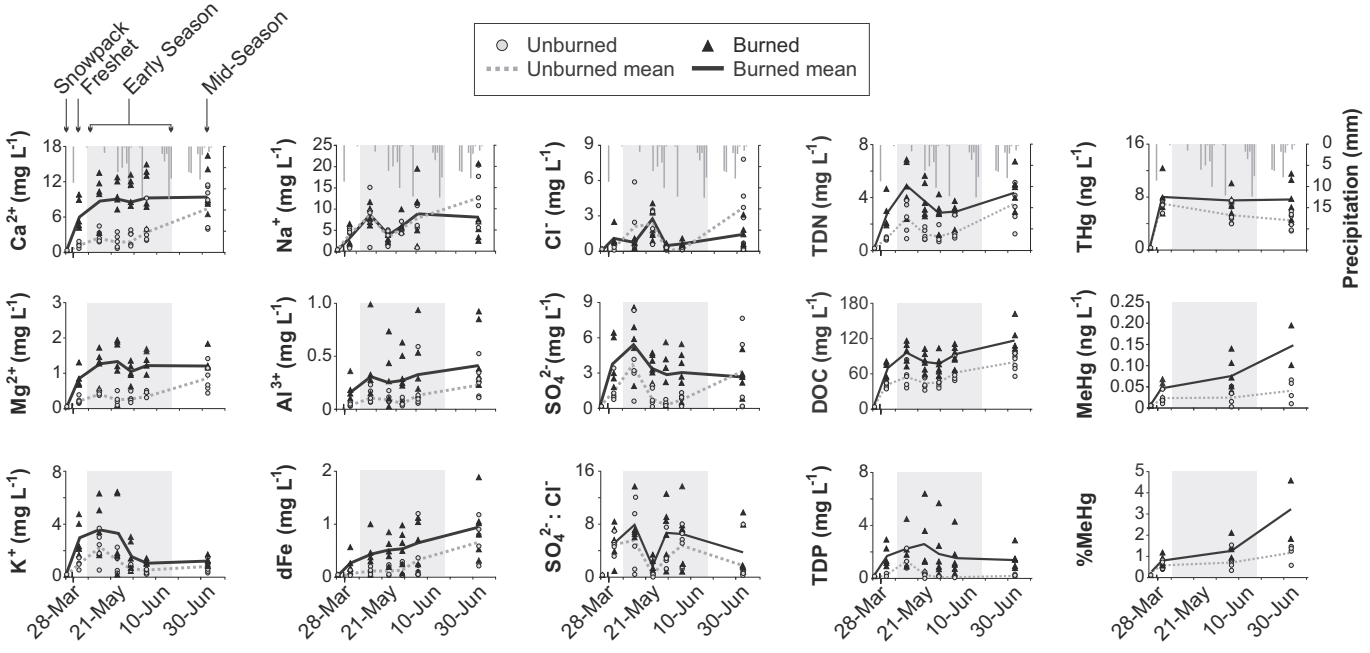

Fig. 7. Concentrations of major ions, dissolved organic carbon (DOC), nutrients (total dissolved nitrogen and phosphorus; TDN, TDP), dissolved total mercury (THg), dissolved methylmercury (MeHg), and percentage of THg in the form of MeHg (%MeHg) in snowpack water (28 March 2016) and peat pore water collected during the freshet (7 May 2016), early season (16 May–6 June 2016, shown in gray), and mid-season (3 July 2016) plotted with daily cumulative precipitation in the top panels. Note ion and nutrient concentrations are in mg L^{-1}, while THg and MeHg concentrations are in ng L^{-1}.

sites, increasing ρ_b with depth occurred in concert with a decrease of both total porosity (ϕ_T) and effective porosity (ϕ_{EFF}) (Fig. 8a-c). Though differences in ϕ_{EFF} were not detected from 0 to 9 cm, ϕ_{EFF} was 52% lower in the burned site at 15 cm ($p = 0.05$, Table S5), and 17% lower at 17 cm. Cumulative pore size distributions (Fig. 8d), derived from volumetric water retention curves (Fig. 8f), were consistent throughout the unburned profile. Additionally, these curves were nearly identical between sites at 5 cm depth where relative pore volume with opening diameter of less than 114 μm was 54% and 56% in the unburned and burned sites, respectively. However, small pores accounted for a higher proportion of the porosity with depth at the burned site. For example, at a depth of 15 cm, nearly 100% of the pores at the burned site have a diameter of 114 μm or less, while at the unburned site, only about 50% of the pores have such diameters (Fig. 8d).

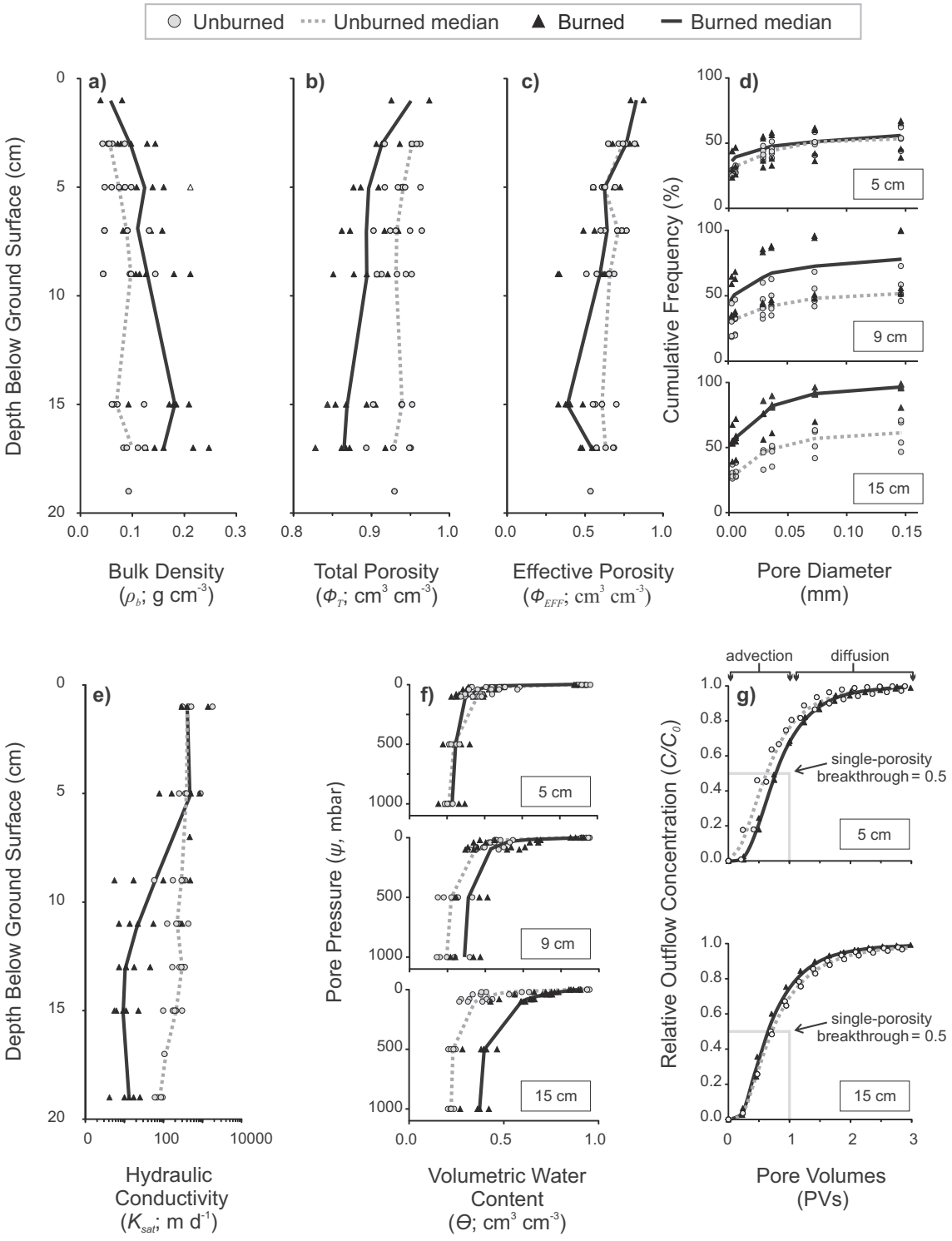

Fig. 8. Physical and hydraulic properties of peat sub-cores collected from the surface 20 cm profile including (a) ρ_b, bulk density, (b) ϕ_T, total porosity, (c) ϕ_{EFF}, effective porosity, (d) K_{sat}, saturated hydraulic conductivity, (e) cumulative % pore size frequency, (f) volumetric soil water retention at different pore pressures, and (g) average chloride breakthrough curves (BTCs) determined by the average parameters from fitting each individual BTC. Note differences in x-axes scales.

Table 1
The derived parameters from fitting the mobile-immobile solute transport model to the observed BTC data for peat sub-cores collected from the moss-covered surface in the burned and unburned sites. Breakthrough curve analyses were performed on two replicate (Rep) sub-cores from each of the burned and unburned sites at both 4–6 cm and 14–16 cm below the ground surface. The velocity (cm min^{-1}) is the average linear pore water velocity. The hydrodynamic dispersion coefficient (cm^2 min^{-1}) is a solute- and media-dependent parameter that describes the lateral spread of a given solute away from the primary advective flux direction. The beta parameter is the proportion of the total porosity that is contributing to advective solute transport. This parameter can be related to the drainable porosity (ϕ_{EFF}) at −100 mb but is not required (McCarter et al., 2019). The omega parameter is a dimensionless mass transfer coefficient describing the movement of a solute between the mobile and immobile porosity. In this case, the omega parameter is only used as a tuning parameter. Goodness of fit is presented as root mean square error (RMSE).

Core	Depth	*Velocity*	*Dispersion*	*Beta*	*Omega*	ϕ_{EFF}	*RMSE*
	[cm]	[cm min^{-1}]	[cm^2 min^{-1}]	[−]	[−]	[−]	[−]
Unburned Rep #1	4–6	0.098	0.100	0.80	0.001	0.62	0.04
Unburned Rep #2	4–6	0.081	0.026	0.75	0.001	0.63	0.04
Burned Rep #1	4–6	0.035	0.016	0.33	0.001	0.55	0.04
Burned Rep #2	4–6	0.105	0.078	0.75	0.001	0.55	0.05
Unburned Rep #1	14–16	0.022	0.010	0.20	0.012	0.57	0.03
Unburned Rep #2	14–16	0.014	0.007	0.13	0.026	0.55	0.03
Burned Rep #1	14–16	0.041	0.017	0.34	0.001	0.39	0.03
Burned Rep #2	14–16	0.010	0.005	0.09	0.017	0.33	0.03

The saturated hydraulic conductivity (K_{sat}; Fig. 8e) was significantly lower at the burned site than the unburned ($p = 0.002$, Table S5), driven by decreases at all depths but with only a significant difference at the 15 cm depth ($p = 0.001$, Table S5). This systematic decrease in K_{sat} drove an overall decrease in the average vertical K_{sat} (*i.e.*, the harmonic mean of a vertical profile; note, linear interpolation of the K_{sat} data was used when no K_{sat} data was present for a given layer) of the burned peat cores (24 ± 7 m day^{-1}) compared to the unburned peat (193 ± 20 m day^{-1}). Differences were also noted between the burned and unburned sites in terms of moisture retention. For example, volumetric soil water retention remained relatively constant in the unburned cores along the entire 20 cm profile at all matric pressures (ψ) (Fig. 8f). Significant differences in volumetric water content (Θ) between sites were not observed until a depth of 9 cm, where median Θ was nominally greater in the burned at $\psi > 0$ mbar and significantly greater at $\psi \geq 500$ mbar. The median Θ differences increased with depth so that at 15 cm, Θ was significantly greater at all $\psi > 0$ mbar (Fig. 8f).

Differences in peat pore structure between the burned and unburned sites were also identified by the Cl^- breakthrough curves (BTCs; Fig. 8g). Breakthrough midpoint ($C/C_0 = 0.5$) occurred before one pore volume in all burned and unburned sub-cores. However, at 5 cm the midpoint of the BTC was reached earlier in the unburned as compared to the burned. In addition, a longer, more gradual tailing (where C/C_0 approaches 1) was observed in the unburned samples. There was no clear distinction between burned and unburned parameters, but variability did increase in burned sub-cores (Table 1). At 15 cm depth, though similar solute detection time (when Cl^- is first detected in the effluent), the variability of derived parameters increased in the burned sub-cores (Table 1). There was clear separation of the curves at ~0.5 pore volumes (Fig. 8g), likely driven by the decreased effective porosity in sub-cores from the burned site (Table 1).

5. Discussion

5.1. Snow cover, frost table depth and runoff flowpaths

The differing snow accumulation in the burned and unburned plateaus (Fig. 3) is attributed to changes resulting from the total combustion of the black spruce canopy due to the wildfire; both directly through subtle differences in snow interception and indirectly, and likely of greater importance, due to its effect on altering wind and energy dynamics (Pomeroy et al., 2008; Gleason et al., 2013). Snow depth is typically assumed to be greater in forested sites impacted by wildfire, often in environments with higher density canopy cover than the comparatively-sparse black spruce forests of the Scotty Creek basin (Smith et al., 2015). However in this study, the loss of canopy from the burned site enabled greater redistribution of snow by wind and altered radiation dynamics, which in combination increased the snowpack density sufficiently that the SWE of the burned site was greater (Fig. 3c) despite having lower mean snow depths (Fig. 3a). The differing snow and energy dynamics between the burned and unburned sites affected the rate and pattern of ground thaw, with the distinction between sites becoming increasingly apparent as the snow-free season progressed (Fig. 5).

The snow cover of the burned site was relatively uniform compared to the unburned site, which contained numerous snow-free tree wells, protruding small trees and branches, and was littered with canopy debris. As a result, the snow surface albedo (Fig. 2) across the burned site remained higher over winter and into the melt period. The higher albedo coupled with lower longwave emittance, both L_{in} and L_{out} (Fig. 2), from the lack of exposed live vegetation delayed the onset of melt relative to the unburned site and, in association with wind-driven snow redistribution, likely contributed to the slightly elevated frost table ruggedness in late May 2016 (Fig. 5). However, the greater transmissivity of the burned canopy enabled a more spatially homogenous K_{in} flux, resulting in a rapid and relatively uniform snow melt (Gleason et al., 2013), followed by a rapid and relatively uniform ground thaw. Although the burned site had a significantly deeper frost table at the end of May 2016 and into the summer months, the greater prevalence of taliks in the unburned site was likely a function of the proximity of the unburned plots to the adjacent channel fen (Fig. 1) and the influence of advective energy contributing to permafrost thaw in this site (Devoie et al., 2019).

Severe burns can reduce the ground surface albedo by 50% or more (Rouse and Kershaw, 1971; Yoshikawa et al., 2001). However, for this low severity burn that yielded minimal ground surface damage beyond singeing, the reduction in albedo was relatively minor (Fig. 2). The combined effect of the reduced albedo and increased insolation due to the loss of canopy led to significantly higher thaw rates at the burned; a difference that became increasingly pronounced as the thaw period progressed (Fig. 4). Moreover, in comparing the spatial patterns of thaw of the two sites, it is apparent that by creating a more uniform, lower ground surface albedo in concert with increasing and uniform insolation, the wildfire dampened spatial variations in ground thaw at the burned site (Fig. 5). Near the mid-point of the growing season, it was evident at the unburned site that unshaded areas had thawed to greater depths, resulting in a spatially variable thaw depth pattern (Fig. 5). The variability in thaw depth reflected the spatial variability observed in snowpack melt and loss during the snowmelt period (Fig. 3d).

Preferential thaw on peat plateaus generates depressions in the frost table and therefore local hydraulic gradients that redistribute subsurface water to the depressions (Wright et al., 2009). The greater soil moisture content of the depressions enables greater conduction of energy from the ground surface to the frost table, thereby maintaining the relatively high thaw rate (Hayashi et al., 2007). These depressions

exhibit threshold behaviour, whereby they function as internally-drained water storage features above the frost table. Once depression storage capacity is exceeded, any additional water is conveyed downslope. Since ground thaw continually adjusts the frost table in the downward direction, frost table depressions can also release water if their depression volume is reduced by thaw of the confining frost table (Fig. 4). As the thaw season progressed, many such thaw depressions coalesced, a process that often transformed the hydrological function of these depressions from subsurface water storage (with intermittent threshold excess runoff) to subsurface water conveyance (Koch et al., 2014). While this process continued in all plots throughout the thaw season, it was more pronounced in the unburned plots; where by late summer networks of deep, meandering subsurface channels had developed (see Late August FT for the unburned site in Fig. 5). The saturated layer occupied deeper, less conductive peat later in the thaw season in the unburned site. The subsurface channels brought about by patchy thaw in the surface ~20 cm of peat in the unburned site enabled the rapid conveyance of water and solutes downslope. This is aided by the redistribution of water from areas of shallower frost table depths to the depressions, which sustained the relatively high water table positions in the latter.

Even during dry periods, the very low drainable porosity of deep peat layers enabled the water table to quickly rise to more surficial peat layers in response to precipitation input, which are highly conductive under unburned conditions. The more efficient drainage of the unburned site, due to the higher hydraulic conductivity at depth, enabled it to remain relatively dry. These dry conditions promote permafrost stability (Wright et al., 2009). The lack of preferential thaw at the burned site greatly reduced the development of subsurface flow channels. As a result of the preferential thaw dynamics and lower hydraulic conductivity in the saturated peat, the burned site was relatively poorly drained and therefore maintained a thicker saturated layer (Fig. 6d). With the loss of tree canopy, reduced evapotranspiration (ET) likely contributed to the wetter condition of the burned, although daily ET losses from undisturbed peat plateaus have been shown to be an order of magnitude lower than daily subsurface runoff (Warren et al., 2018). The feedbacks between reduced ET, decreased hydraulic conductivity at depth, and uniform thaw decrease water conveyance from burned permafrost peatlands.

5.2. Peat physical properties and hydraulic response

The physical properties of peat changed significantly with exposure to the low severity wildfire, affecting the hydraulic properties of these soils despite the lack of considerable ground surface disturbance. Given that snowmelt accounted for approximately 40% of the 2016 precipitation, and the average thaw depths in both the burned and unburned sites had reached approximately 20 cm by the completion of snowmelt, the conveyance of a significant proportion of annual precipitation was influenced by the hydraulics of the upper 20 cm of peat. During the snowmelt period, the hydraulic conductivity between the ground surface and frost table was uniformly high at the unburned site but was one to two orders of magnitude lower at the burned site by 10 cm below the ground surface. Throughout the 20 cm profile of unburned peat, median bulk density (ρ_b), total porosity (ϕ_T), effective porosity (ϕ_{EFF}) and pore size distributions (Fig. 8a-c and e) were similar to values determined in other northern peatlands (Hayward and Clymo, 1982; Hoag and Price, 1997; Quinton et al., 2008; Holden, 2009; Rezanezhad et al., 2016). In contrast, the higher median ρ_b in the burned peat at depths as shallow as 3 cm, and an associated reduction in ϕ_T, suggests peat compression and consolidation occurred. This compression of near-surface peat is further supported by the fact that *Sphagnum* moss was still identifiable at the ground surface, suggesting that the surface peat did not completely burn. Extreme heating of surface vegetation that destroys near-surface plant cellular structure, including the *Sphagnum* capitula and water-holding hyaline cells (Sherwood et al., 2013) as reflected by the significant change in the small pores, likely contributed to the consistently low soil moisture in shallow peat at the burned site (Fig. 8f), as compared to the unburned site. This drying and densification of the near-surface peat cause shrinkage and compression (Hayward and Clymo, 1982; McCarter and Price, 2014; Golubev and Whittington, 2018) that vertically displace the ground surface downward, resulting in deeper, denser peat of lower hydraulic conductivity closer to the surface. Since the rate of horizontal runoff transmission was limited by the saturated hydraulic conductivity, the fire-induced thinning of the near-surface zone of highly-conductive peat slowed the movement of water on the burned plateau and likely resulted in a longer residence time for water and solutes.

Although the combustion of surface vegetation converts low density organic matter into higher density ash and char (Redding and Devito, 2016), it is unlikely, given the low severity of this fire event in terms of the sustained ground surface damage, that plant tissues were transformed in this way at depths much greater than 5 cm (Debano, 2000). Rather, the physical changes observed at peat depths greater than 5 cm (Fig. 8) suggest that dense ash and other particulates generated by the wildfire (Redding and Devito, 2016) were translocated from the surface and incorporated into inter-particle pore spaces, thereby increasing the peat ρ_b. Not only would this increase the aggregate volume of smaller pore sizes as we observed, it would also decrease the ϕ_{EFF}, supported by the results of the BTC sub-cores at both burned depths (Fig. 8g; Tables 1, S5), and provide greater surface area of the ash-altered peat (Stoof et al., 2010). This is further reinforced by the elevated cation concentrations observed in pore waters at such depths sampled during the early- and mid-seasons at the burned site (Fig. 7, Table S4), which indicate the presence of wildfire-delivered ash content (Flannigan et al., 2009). These physical changes prevent rapid percolation and promote moisture retention (Hayward and Clymo, 1982; Nimmo, 2004), thereby increasing the capacity of the peat to store water and solutes, rather than facilitating conveyance.

Smaller clogged and compressed pores in peat impacted by wildfire occupied a greater proportion of the peat profile below 5 cm as compared to the unburned site (Fig. 8e). Consequently, the fire-affected peat had not only greater moisture retention and storage, but also triggered an amplified water table response to precipitation (*e.g.*, Event A response; Fig. 6a). This event induced three abrupt soil moisture increases at the burned site that gradually lessened over time and cumulative water table rises resulting in a maximum increase of 8 cm. The lower K_{sat} below 5 cm at the burned site (Fig. 8d) resulted in a proportionately lower rate of horizontal runoff through the saturated layer, causing greater temporary saturated storage and therefore a higher water table position than prior to the event (Fig. 6d). In contrast, the highly conductive peat at the unburned site enabled precipitation to rapidly percolate through the peat column and efficiently direct runoff and thermal energy along preferential flowpaths. The contrasting hydraulic response, and fire-induced feedbacks similar to those identified in northern peatlands affected by climate-mediated and land use disturbances (Whittington and Price, 2006; Waddington et al., 2015), illustrates that the burn-affected peat maintains both higher soil moisture above the water table, and a thicker saturated layer, thereby increasing both saturated and unsaturated soil water residence time.

The mechanisms responsible for the field hydraulic response are reflected in the shape of the BTCs of the collected peat cores. However, there was no consistent pattern between burned and unburned cores in the derived parameters, likely due to the observed large variability of solute transport parameters in peat (McCarter et al., 2020). Limited change in transport parameters is common in peat, as small changes to these parameters (well within the observed variability in this study) can indicate larger physical changes (McCarter et al., 2019). In any case, the results here indicate that a more systematic approach to determining how wildfire impacts solute transport processes in peat and peatlands is required and remains a critical gap in our knowledge.

The transport and dispersion of water and solute through soil is dependent on average pore water velocity, which is influenced by pore size (Bear, 1972; Holden, 2009) and pore structures (Rezanezhad et al., 2016; McCarter et al., 2020). The complex dual-porosity structure of peat, with both mobile and immobile pores, resulted in the BTC midpoint (where $C/C_0 = 0.5$) to be reached before the passage of one pore volume in all sub-cores depths from both the burned and unburned sites. However, varying detection time and curve shape at each depth distinguished the dominant pore structures of the near-surface (5 cm) peat from the deeper (15 cm) peat and highlighted the impacts of the low-severity burn on flow. The ϕ_{EFF} decreased and variability of the beta parameter (the proportion of active porosity relative to total porosity) increased in both burned samples, with the greatest changes in the deeper soil layers (Table 1). The change to these mobile porosity metrics within the 15 cm burned peat (Table S5) is consistent with the addition of particulates (*e.g.*, ash, char) decreasing the porosity available for transport (Stoof et al., 2010).

In the upper peat, the overall change was not as substantial as that observed for the deep peat, partly due to a greater abundance of large pores that are able to convey these particulates of ash and char to greater depths where they become entrained. The clear decrease in ϕ_{EFF} has important implications for both solute source and reaction time at different depths, as fine ash and char particulates become a potential source of additional solutes while concomitantly reducing runoff rates and increasing residence times. In turn, cation exchange and nutrient leaching into plateau runoff are enhanced while allowing greater time for biogeochemical reactions to occur.

5.3. Seasonal runoff water chemistry

The clear increase in pore water solute concentrations at burned sites during the early- and mid-season, but lack of response in the snowpack, points to the role of increasing soil-water interaction and changes to chemical composition within peat soils in the biogeochemical response to wildfire. We suggest that increased waterlogging and water residence time within soils is consistent with these results, similar to the observations of altered geochemical dynamics in Arctic rivers draining basins undergoing permafrost degradation (Frey and McClelland, 2009). The observed reduction in pore sizes and changes in solute transport processes in the burned soils is likely coupled with the deposition of ion-rich ash on the peat surface and its translocation downwards into the peat matrix, contributing to the observed changes in peat pore water chemistry. The effect of ash translocation on cationic pore water loads is likely further amplified by the high cation exchange capacity, and thus potential for cation retention from translocated ash and re-release during high-flow events, in peat soils (Certini, 2005).

Similar to the ionic response, the observed increases in nutrient (TDN, TDP) and organic carbon (DOC) concentrations are consistent with increased water residence time in soils. Following this low-severity burn with minimal ground surface disturbance, the nutrient enrichment (Fig. 7) detected in pore water was likely further enhanced by decreased nutrient uptake due to loss of vegetation and a subsequent release of nutrients through leaching from burned organic matter. Although typically minimal in overall contributions to total dissolved loads of nitrogen and phosphorus, extreme heating of organic matter produces NH_4^+, NO_3^-, and PO_4^{3-} and converts labile carbon to more recalcitrant, less biodegradable forms that may have longer residence times in soil solution (Olefeldt et al., 2013, 2014; Parham et al., 2013). Degrading soot (condensed volatiles) and char (solid organic residue) can similarly migrate downward into the peat matrix (Certini, 2005; Preston and Schmidt, 2006; Flannigan et al., 2009; Olefeldt et al., 2014), transferring nutrients back into the soil solution.

Because of the affinity between Hg and organic matter, DOC and THg concentrations are often strongly related (Driscoll et al., 1995). Given the observed connection between increased Hg and organic matter in dissolved and particulate forms from thawing permafrost basins (Schuster et al., 2011), permafrost disturbance due to wildfire may similarly impact Hg partitioning from the solid phase peat and the subsequent mobility in pore water. Through anaerobic respiration of organic matter, predominantly sulfate-reducing bacteria transform Hg into toxic methylmercury (MeHg), which is dependent on the availability of THg, labile carbon (DOC) and terminal electron acceptors including SO_4^{2-}, and limited by the activity of SO_4^{2-} reducing bacteria, which is largely temperature-dependent (Branfireun et al., 1999; Tjerngren et al., 2012; Gilmour et al., 2013). Greater dissolved MeHg and percent of dissolved THg in the form of MeHg (%MeHg) in the burned site pore water, particularly in the deeper samples collected during the warmer mid-season months where greater reducing conditions exist (Gordon et al., 2016), DOC concentrations were elevated and SO_4^{2-} was still present, is consistent with the increased microbial reduction of SO_4^{2-} throughout much of the thaw season. This process likely drove the difference in MeHg concentrations between the burned and unburned sites.

Increasing ground thaw in the burned site beyond the anticipated frost table depth based on the observed position in the unburned site, particularly later in the thaw season (*i.e.*, Fig. 4), would enable permafrost thaw and the subsequent release of water and solute from long-term storage (Shur and Jorgenson, 2007; Koch et al., 2014; Brown et al., 2015; Gordon et al., 2016). At the same time, the relatively slow subsurface drainage from burned sites increases the time available for solute leaching and biogeochemical reactions to occur. The effects of wildfire on pore water chemistry appear to be seasonally variable, driven by hydrological mechanisms and influenced by the fire-induced changes to peat pore structure and hydraulic properties. Elevated ions, nutrients and mercury in peat pore water of the burn-affected plateau during the spring freshet and through to early June have the potential to increase loading to downstream aquatic ecosystems. Although there is a clear increase in the dissolved pore water solutes (Fig. 7), the exponential decline in hydraulic conductivity with depth, which is exacerbated by the low severity burn, will induce preferential lateral flushing of the near surface layers, rather than flushing of the deeper (*i.e.*, 15 cm) peats and the movement of these solutes may be limited in these peatlands post-burn. In addition to the temporal variation in the fire-impacted and unaffected sites, spatial variation in fire patterns likely contributed to variability in pore water chemistry on the burned peat plateaus. Although there was generally minimal damage to the peat surface on the burned plateaus with moss and lichen remaining identifiable, soil combustion was apparently enhanced around the base of trees, resulting in the formation of burn depressions. The cation content of pore water in closer proximity to these tree-centred burn depressions is likely enhanced and warrants further investigation. However, proximity to burn depressions was not considered in the sampling approach in this study. Despite the elevated pore water solute concentrations in peatlands that have experienced a low severity fire in terms of ground surface damage and singeing, the mobilization, downstream transport and introduction of these solutes to aquatic systems are unknown. The interplay between peat hydraulic properties and solute chemistry, and the variation in wildfire effects with depth, illustrate the complex and dynamic processes that control water and solute movement in these landscapes.

6. Conclusions

Low-severity wildfires of peat-dominated plateau-wetland complexes in the discontinuous permafrost landscape significantly affect the thermal, hydrological and biogeochemical dynamics of this environment. The reduction of the black spruce canopy and burning of the shallow surface organic matter catalyzes a series of feedbacks affecting the peat hydraulic properties, the energy dynamics of the supra-permafrost layer and the underlying permafrost, as well as the routing and storage of water, which ultimately alters the geochemistry of pore water that can be exported as runoff from elevated peat plateaus. The dramatic changes

range from small scale effects on peat pore structure and physical properties to large scale impacts on snowmelt dynamics and seasonal permafrost thaw, suggesting that wildfires of modest severity that do not significantly disturb the peat surface have the potential to trigger significant hydrological and biogeochemical effects. The elevated solute concentrations in peat pore water of the wildfire-impacted site and the seasonal and flow-driven trends in these concentrations suggest that the observed biogeochemical effects are largely controlled by physically-induced changes in hydrology. Hydraulic feedback mechanisms catalyzed by the fire resulting in longer pore water residence times coupled with the mobilization of solutes in the form of translocated ash and char particulates demonstrate the interrelated nature of hydrological mechanisms and biogeochemical fluxes in this landscape. Triggered by altered snowmelt and thermal dynamics, deeper and more rapid thaw further alters hydrology, residence time, and soil-water interactions. Further research is required to examine the likely episodic nature of solute mobilization as compared to storage resulting from the burn-induced changes in peat hydraulic properties on flowpaths coupled with the effects of solute and contaminant loading resulting from low-severity wildfires to adjacent wetlands and aquatic environments downstream of the hydrologically-connected, cascading landscape features of the discontinuous permafrost zone. Given the modest severity of this wildfire in terms of ground surface disturbance and singeing, yet considerable hydrological, thermal and biogeochemical response, quantifying the length of the response time and the trajectory of these dynamics will be important for better understanding the long-term effects of fire in this landscape. Further research is similarly required to comparatively examine the holistic impacts of high severity fires in this mosaicked landscape, with thick organic matter deposits. As wildfire acts to accelerate permafrost thaw in this rapidly-changing environment, with plateaus transitioning to wetlands, assessment of the trajectory of fire-impacted features in the discontinuous permafrost landscape of northwestern Canada and the circumpolar subarctic is warranted.

CRediT authorship contribution statement

Caren Ackley: Conceptualization, Methodology, Formal analysis, Investigation, Writing – original draft, Writing – review & editing, Visualization. **Suzanne E. Tank:** Conceptualization, Methodology, Formal analysis, Resources, Supervision, Project administration, Funding acquisition, Writing – original draft, Writing – review & editing, Visualization. **Kristine M. Haynes:** Formal analysis, Writing – original draft, Writing – review & editing, Visualization. **Fereidoun Rezanezhad:** Methodology, Resources, Writing – original draft, Writing – review & editing, Visualization. **Colin McCarter:** Methodology, Formal analysis, Writing – original draft, Writing – review & editing, Visualization. **William L. Quinton:** Conceptualization, Methodology, Investigation, Resources, Supervision, Project administration, Funding acquisition, Writing – original draft, Writing – review & editing, Visualization.

Declaration of competing interest

The authors declare that they have no known competing financial interests or personal relationships that could have appeared to influence the work reported in this paper.

Acknowledgements

The authors wish to thank the offices of the Liidlii Kue First Nation, the Jean-Marie River First Nation, and the Dehcho First Nations for their support of both the Scotty Creek Research Station and this project. We also gratefully acknowledge Polar Knowledge Canada for their financial support for this study provided through grants 1516-107 and 1617-0009. We would like to acknowledge the Canada Excellence Research Chair program in Ecohydrology at the University of Waterloo for providing the lab supplies for the flow-through reactor experiment. We also wish to thank Clara Ackley for her dedicated work as a Research Assistant, as well as Michael Braverman, Olivia Carpino, Ryan Connon, Elise Devoie, Geoffrey Kershaw, Joelle Langford, Alex MacLean, Elzbieta Mastej, Elyse Mathieu, Riley Mills, Ashley Rudy, Katherine Standen, Lindsay Stone, Marianne Vandergriendt, Meagan Warkentin, Becca Warren and Nick Wilson for their assistance throughout this study. We thank the three reviewers for their constructive comments.

Appendix A. Supplementary data

Supplementary data to this article can be found online at https://doi.org/10.1016/j.scitotenv.2021.146841.

References

American Public Health Association, 2017. Standard Methods for the Examination of Water and Wastewater.
Bear, J., 1972. Dynamics of Fluids in Porous Media. Dover Publications, Inc., New York.
Beilman, D.W., Robinson, S.D., 2003. Peatland permafrost thaw and landform type along a climate gradient. In: Phillips, M., Springman, S.M., Arenson, L.U. (Eds.), Proceedings of the Eighth International Conference on Permafrost. vol. 1. Balkema, Zurich, pp. 61–65.
Branfireun, B.A., Roulet, N.T., Kelly, C.A., Rudd, J.W.M., 1999. In situ sulphate stimulation of mercury methylation in a boreal peatland: toward a link between acid rain and methylmercury contamination in remote environments. Glob. Biogeochem. Cycles 13 (3), 743–750. https://doi.org/10.1029/1999GB900033.
Brown, D.R.N., Jorgenson, M.T., Douglas, T.A., Romanovsky, V.E., Kielland, K., Hiemstra, C., Euskirchen, E.S., Ruess, R.W., 2015. Interactive effects of wildfire and climate on permafrost degradation in Alaskan lowland forests. Journal of Geophysical Research G: Biogeosciences 120 (8), 1619–1637. https://doi.org/10.1002/2015JG003033.
Camill, P., 2005. Permafrost thaw accelerates in boreal Peatlands during Late-20th Century climate warming. Clim. Chang. 68, 135–152.
Certini, G., 2005. Effects of fire on properties of forest soils: a review. Oecologia 143 (1), 1–10. https://doi.org/10.1007/s00442-004-1788-8.
Connon, R., Devoie, É., Hayashi, M., Veness, T., Quinton, W., 2018. The Influence of Shallow Taliks on Permafrost Thaw and Active Layer Dynamics in Subarctic Canada. Journal of Geophysical Research, Earth Surface, pp. 1–17 https://doi.org/10.1002/2017JF004469.
Connon, R.F., Quinton, W.L., Craig, J.R., Hayashi, M., 2014. Changing hydrologic connectivity due to permafrost thaw in the lower Liard River valley, NWT, Canada. Hydrol. Process. 28, 4163–4178. https://doi.org/10.1002/hyp.10206.
Debano, L.F., 2000. The role of fire and soil heating on water repellency in wildland environments: a review. J. Hydrol. 231–232, 195–206. https://doi.org/10.1016/S0022-1694(00)00194-3.
Development Core Team, R., 2018. R: A Language and Environment for Statistical Computing. R Foundation for Statistical Computing, Vienna, Austria.
Devoie, É.G., Craig, J.R., Quinton, W.L., Connon, R.F., 2019. Taliks: a tipping point in discontinuous permafrost degradation in peatlands. Water Resour. Res. 55 (11), 9838–9857.
Driscoll, C.T., Blette, V., Yan, C., Schofield, C.L., Munson, R., Holsapple, J., 1995. The role of dissolved organic carbon in the chemistry and bioavailability of mercury in remote Adirondack lakes. Water Air Soil Pollut. 80, 499–508.
Environment Canada, 2020. Historical climate data. (2020). http://climate.weather.gc.ca/historical_data/search_historic_data_e.html.
Flannigan, M., Stocks, B., Turetsky, M., Wotton, M., 2009. Impacts of climate change on fire activity and fire management in the circumboreal forest. Glob. Chang. Biol. 15, 549–560. https://doi.org/10.1111/j.1365-2486.2008.01660.x.
Frey, K.E., McClelland, J.W., 2009. Impacts of permafrost degradation on arctic river biogeochemistry. Hydrol. Process. 23, 169–182. https://doi.org/10.1002/hyp.7196.
van Genuchten, M.T., Wagenet, R.J., 1989. Two-site/two-region models for pesticide transport and degradation: theoretical development and analytical solutions. Soil Sci. Soc. Am. J. 53, 1303–1310. https://doi.org/10.2136/sssaj1989.03615995005300050001x.
Gibson, C.M., Chasmer, L.E., Thompson, D.K., Quinton, W.L., Flannigan, M.D., Olefeldt, D., 2018. Wildfire as a major driver of recent permafrost thaw in boreal peatlands. Nat. Commun. 9 (1). https://doi.org/10.1038/s41467-018-05457-1.
Gilmour, C.C., Podar, M., Bullock, A.L., Graham, A.M., Brown, S.D., Somenahally, A.C., Johs, A., Hurt, R.A., Bailey, K.L., Elias, D.A., 2013. Mercury methylation by novel microorganisms from new environments. Environ. Sci. Technol. 47 (20), 11810–11820. https://doi.org/10.1021/es403075t.
Gleason, K.E., Nolin, A.W., Roth, T.R., 2013. Charred forests increase snowmelt: effects of burned woody debris and incoming solar radiation on snow ablation. Geophys. Res. Lett. 40, 4654–4661. https://doi.org/10.1002/grl.50896.
Golubev, V., Whittington, P., 2018. Effects of volume change on the unsaturated hydraulic conductivity of Sphagnum moss. J. Hydrol. 559, 884–894. https://doi.org/10.1016/j.jhydrol.2018.02.083.
Gordon, J., Quinton, W., Branfireun, B.A., Olefeldt, D., 2016. Mercury and methylmercury biogeochemistry in a thawing permafrost wetland complex, Northwest Territories, Canada. Hydrol. Process. 30 (20), 3627–3638. https://doi.org/10.1002/hyp.10911.
de Groot, W.J., Cantin, A.S., Flannigan, M.D., Soja, A.J., Gowman, L.M., Newbery, A., 2013. A comparison of Canadian and Russian boreal fire regimes. For. Ecol. Manag. 294, 23–34.
Hamlin, L., Pietroniro, A., Prowse, T., Soulis, R., Kouwen, N., 1998. Application of indexed snowmelt algorithms in a northern wetland regime. Hydrol. Process. 12, 1641–1657.

Hanes, C.C., Wang, X., Jain, P., Parisien, M.-A., Little, J.M., Flannigan, M.D., 2019. Fire-regime changes in Canada over the last half century. Can. J. For. Res. 49 (3). https://doi.org/10.1139/cjfr-2018-0293.

Harden, J.W., Manies, K.L., Turetsky, M.R., Neff, J.C., 2006. Effects of wildfire and permafrost on soil organic matter and soil climate in interior Alaska. Glob. Chang. Biol. 12, 2391–2403. https://doi.org/10.1111/j.1365-2486.2006.01255.x.

Hayashi, M., Goeller, N., Quinton, W.L., Wright, N., 2007. A simple heat-conduction method for simulating the frost-table depth in hydrological models. Hydrol. Process. 21, 2610–2622. https://doi.org/10.1002/hyp.6792.

Haynes, K.M., Connon, R.F., Quinton, W.L., 2018. Permafrost thaw induced drying of wetlands at Scotty Creek, NWT, Canada. Environ. Res. Lett. 13 (11), 114001. https://doi.org/10.1088/1748-9326/aae46c.

Hayward, P.M., Clymo, R.S., 1982. Profiles of water content and pore size in Sphagnum and peat, and their relation to peat bog ecology. Proc. R. Soc. B Biol. Sci. 215 (1200), 299–325. https://doi.org/10.1098/rspb.1982.0044.

Heginbottom, J.A., Dubreuil, M.A., Harker, P.A., 1995. Canada permafrost. National Atlas of Canada, 5th ed. Natural Resources Canada, Ottawa, Ont., Canada.

Helbig, M., Pappas, C., Sonnentag, O., 2016. Permafrost thaw and wildfire: equally important drivers of boreal tree cover changes in the Taiga Plains, Canada. Geophys. Res. Lett. 43, 1598–1606.

Hoag, R.S., Price, J.S., 1997. The effects of matrix diffusion on solute transport and retardation in undisturbed peat in laboratory columns. J. Contam. Hydrol. 28, 193–205.

Holden, J., 2009. Flow through macropores of different size classes in blanket peat. J. Hydrol. 364, 342–348. https://doi.org/10.1016/j.jhydrol.2008.11.010.

Holloway, J., Lewkowicz, A., 2020. Half a century of discontinuous permafrost persistence and degradation in western Canada. Permafr. Periglac. Process. 31, 85–96.

Holloway, J., Lewkowicz, A., Douglas, T., Li, X., Turetsky, M., Baltzer, J., Jin, H., 2020. Impacts of wildfire on permafrost landscapes: a review of recent advances and future prospects. Permafr. Periglac. Process., 1–12 https://doi.org/10.1002/ppp.2048.

Huang, K., Toride, N., Van Genuchten, M.T., 1995. Experimental investigation of solute transport in large, homogeneous and heterogeneous, saturated soil columns. Transp. Porous Media 18 (3), 283–302. https://doi.org/10.1007/BF00616936.

IUSS Working Group WRB, 2015. World reference base for soil resources 2014, update 2015 International Soil Classification System for naming soils and creating legends for soil maps. World Soil Resources Reports No. 106. FAO, Rome.

Jafarov, E.E., Romanovsky, V.E., Genet, H., Mcguire, A.D., Marchenko, S.S., 2013. The effects of fire on the thermal stability of permafrost in lowland and upland black spruce forests of interior Alaska in a changing climate. Environ. Res. Lett. 8, 1–11. https://doi.org/10.1088/1748-9326/8/3/035030.

Jorgenson, M.T., Osterkamp, T.E., 2005. Response of boreal ecosystems to varying modes of permafrost degradation. Can. J. For. Res. 35, 2100–2111.

Jorgenson, M.T., Romanovsky, V., Harden, J., Shur, Y., O'Donnell, J., Schuur, E.A.G., Kanevskiy, M., Marchenko, S., 2010. Resilience and vulnerability of permafrost to climate change. Can. J. For. Res. 40 (7), 1219–1236. https://doi.org/10.1139/X10-060.

Kasischke, E., Verbyla, D., Rupp, T., McGuire, D., Murphy, K.A., Jandt, R., Barnes, J., Hoy, E., Duffy, P., Calef, M., 2010. Alaska's changing fire regime—implications for the vulnerability of its boreal forests. Can. J. For. Res. 40 (7), 1313–1324.

Keeley, J.E., 2009. Fire intensity, fire severity and burn severity: a brief review and suggested usage. Int. J. Wildland Fire 18 (1), 116–126.

Kettridge, N., Humphrey, R.E., Smith, J.E., Lukenbach, M.C., Devito, K.J., Petrone, R.M., Waddington, J.M., 2014. Burned and unburned peat water repellency: implications for peatland evaporation following wildfire. J. Hydrol. 513, 335–341. https://doi.org/10.1016/j.jhydrol.2014.03.019.

Kleimeier, C., Rezanezhad, F., Van Cappellen, P., Lennartz, B., 2017. Influence of pore structure on solute transport in degraded and undegraded fen peat soils. Mires and Peat https://doi.org/10.19189/MaP.2017.OMB.282.

Koch, J.C., Kikuchi, C.P., Wickland, K.P., Schuster, P., 2014. Runoff sources and flow paths in a partially burned, upland boreal catchment underlain by permafrost. Water Resour. Res. 50, 8141–8158. https://doi.org/10.1002/2013WR014222.Received.

Kokelj, S.V., Palmer, M.J., Lantz, T.C., Burn, C.R., 2017. Ground temperatures and Permafrost Warming from Forest to Tundra, Tuktoyaktuk Coastlands and Anderson Plain, NWT, Canada. Permafr. Periglac. Process. 28 (3), 543–551.

Kwong, Y.T.J., Gan, T.Y., 1994. Northward migration of permafrost along the Mackenzie highway and climatic warming. Clim. Chang. 26 (4), 399–419. https://doi.org/10.1007/BF01094404.

Lenth, R.V., 2020. Emmeans: Estimated Marginal Means, aka Least-squares Means. 1.4.4 ed. .

Lindsay, J.B., 2016. Whitebox GAT: a case study in geomorphometric analysis. Comput. Geosci. 95, 75–84. https://doi.org/10.1016/j.cageo.2016.07.003.

Littlefair, C.A., Tank, S.E., 2018. Biodegradeability of thermokarst carbon in a till-associated, glacial margin landscape: the case of the Peel Plateau, NWT, Canada. J. Geophys. Res. Biogeosci. 123, 3293–3307.

McCarter, C.P.R., Price, J.S., 2014. Ecohydrology of Sphagnum moss hummocks: mechanisms of capitula water supply and simulated effects of evaporation. Ecohydrology 7 (1), 33–44. https://doi.org/10.1002/eco.1313.

McCarter, C.P.R., Rezanezhad, F., Gharedaghloo, B., Price, J.S., Van Cappellen, P., 2019. Transport of chloride and deuterated water in peat: the role of anion exclusion, diffusion, and anion adsorption in a dual porosity organic media. J. Contam. Hydrol. 225, 103497. https://doi.org/10.1016/j.jconhyd.2019.103497.

McCarter, C.P.R., Rezanezhad, F., Quinton, W.L., Gharedaghloo, B., Lennartz, B., Price, J., Connon, R., Van Cappellen, P., 2020. Pore-scale controls on hydrological and geochemical processes in peat: implications on interacting processes. Earth Sci. Rev. 207, 103227. https://doi.org/10.1016/j.earscirev.2020.103227.

McClymont, A.F., Hayashi, M., Bentley, L.R., Christensen, B.S., 2013. Geophysical imaging and thermal modeling of subsurface morphology and thaw evolution of discontinuous permafrost. J. Geophys. Res. Earth Surf. 118 (3), 1826–1837. https://doi.org/10.1002/jgrf.20114.

Meteorological Service of Canada (MSC), 2012. National Climate Data Archive of Canada. Environment Canada, Dorval, Quebec, Canada.

Mueller, D.K., Spahr, N.E., 2005. Water-quality, streamflow, and ancillary data for nutrients in streams and rivers across the nation. 1992–2001: U.S. Geological Survey Data Series Report 152 http://pubs.usgs.gov/ds/2005/152/.

Nimmo, J.R., 2004. Porosity and pore size distribution. Encyclopedia of Soils in the Environment. 3, pp. 295–303. https://doi.org/10.1016/B978-0-12-409548-9.05265-9.

Nossov, D.R., Jorgenson, M.T., Kielland, K., Kanevskiy, M.Z., 2013. Edaphic and microclimatic controls over permafrost response to fire in interior Alaska. Environ. Res. Lett. 8, 035013.

Olefeldt, D., Turetsky, M.R., Blodau, C., 2013. Altered composition and microbial versus UV-mediated degradation of dissolved organic matter in boreal soils following wildfire. Ecosystems 16 (8), 1396–1412. https://doi.org/10.1007/s10021-013-9691-y.

Olefeldt, D., Persson, A., Turetsky, M.R., 2014. Influence of the permafrost boundary on dissolved organic matter characteristics in rivers within the Boreal and Taiga plains of western Canada. Environ. Res. Lett. 9, 1–9. https://doi.org/10.1088/1748-9326/9/3/035005.

Parham, L.M., Prokushkin, A.S., Pokrovsky, O.S., Titov, S.V., Grekova, E., Shirokova, L.S., McDowell, W.H., 2013. Permafrost and fire as regulators of stream chemistry in basins of the Central Siberian Plateau. Biogeochemistry 116, 55–68. https://doi.org/10.1007/s10533-013-9922-5.

Pomeroy, J., Ellis, C., Rowlands, A., Essery, R., Hardy, J., Link, T., Marks, D., Sicart, J.E., 2008. Spatial variability of shortwave irradiance for snowmelt in forests. J. Hydrometeorol. 9 (6), 1482–1490. https://doi.org/10.1175/2008JHM867.1.

Preston, C.M., Schmidt, M.W.I., 2006. Black (pyrogenic) carbon: a synthesis of current knowledge and uncertainties with special consideration of boreal regions. Biogeosciences 3 (4), 397–420. https://doi.org/10.5194/bg-3-397-2006.

Price, J.S., Whittington, P.N., 2010. Water flow in Sphagnum hummocks: Mesocosm measurements and modelling. J. Hydrol. 381, 333–340. https://doi.org/10.1016/j.jhydrol.2009.12.006.

Quinton, W., Berg, A., Braverman, M., Carpino, O., Chasmer, L., Connon, R., Craig, J., Devoie, É., Hayashi, M., Haynes, K., Olefeldt, D., Pietroniro, A., Rezanezhad, F., Schincariol, R., Sonnentag, O., 2019. A synthesis of three decades of hydrological research at Scotty Creek, NWT, Canada. Hydrol. Earth Syst. Sci. 23, 2015–2039. https://doi.org/10.5194/hess-23-2015-2019.

Quinton, W.L., Hayashi, M., 2005. The flow and storage of water in the wetland-dominated Central Mackenzie River basin: recent advances and future directions. Special issue of the Canadian water resources association journal on predicting ungauged streamflow in the Mackenzie Valley: today's techniques & tomorrow's solutions. International Decade for Predictions in Ungauged Basins Yellowknife, Northwest Territories, Canada, March 8–9, 2004, pp. 45–66.

Quinton, W.L., Hayashi, M., Carey, S.K., 2008. Peat hydraulic conductivity in cold regions and its relation to pore size and geometry. Hydrol. Process. 22, 2829–2837. https://doi.org/10.1002/hyp.

Rajendran, A., Kariwala, V., Farooq, S., 2008. Correction procedures for extra-column effects in dynamic column breakthrough experiments. Chem. Eng. Sci. 63 (10), 2696–2706. https://doi.org/10.1016/j.ces.2008.02.023.

Redding, T.E., Devito, K.J., 2016. Particle densities of wetland soils in northern Alberta, Canada. Canadian Journal of Soil Science (February 2006), 57–61 https://doi.org/10.4141/S05-061.

Rezanezhad, F., Price, J.S., Craig, J.R., 2012. The effects of dual porosity on transport and retardation in peat: a laboratory experiment. Can. J. Soil Sci. 92 (5), 723–732. https://doi.org/10.4141/cjss2011-050.

Rezanezhad, F., Price, J.S., Quinton, W.L., Lennartz, B., Milojevic, T., Van Cappellen, P., 2016. Structure of peat soils and implications for water storage, flow and solute transport: a review update for geochemists. Chem. Geol. 429, 75–84. https://doi.org/10.1016/j.chemgeo.2016.03.010.

Richter-Menge, J., Overland, J.E., Mathis, J.T., Osborne, E., 2017. Arctic Report Card 2017. available at. http://www.arctic.noaa.gov/Report-Card.

Robinson, S.D., 2002. Peatlands of the Mackenzie Valley: permafrost, fire, and carbon accumulation. In: Yu, Z.C. (Ed.), Long-Term Dynamics. Proc. of Int. Workshop on Carbon Dynamics of Forested Peatlands: Knowledge Gaps, Uncertainty and Modelling Approaches. 23–24 March, 2001, Edmonton, Canada, pp. 21–24 et al.

Rouse, W.R., Kershaw, K.A., 1971. The effects of burning on the heat and water regimes of lichen-dominated subarctic surfaces. Arct. Alp. Res. 3 (4), 291–304 Available at:. http://www.jstor.org.

Sappington, J.M., Longshore, K.M., Thompson, D.B., 2007. Quantifying landscape ruggedness for animal habitat analysis: a case study using Bighorn sheep in the Mojave Desert. J. Wildl. Manag. 71 (5), 1419–1426. https://doi.org/10.2193/2005-723.

Schuster, P.F., Striegl, R.G., Aiken, G.R., Krabbenhoft, D.P., Dewild, J.F., Butler, K., Kamark, B., Dornblaser, M., 2011. Mercury export from the Yukon River basin and potential response to a changing climate. Environ. Sci. Technol. 45, 9262–9267. https://doi.org/10.1021/es202068b.

Sherwood, J.H., Kettridge, N., Thompson, D.K., Morris, P.J., Silins, U., Waddington, J.M., 2013. Effect of drainage and wildfire on peat hydrophysical properties. Hydrol. Process. 27 (13), 1866–1874. https://doi.org/10.1002/hyp.9820.

Shur, Y., Hinkel, K., Nelson, F., 2005. The transient layer: implications for geocryology and climate-change science. Permafr. Periglac. Process. Vol. 16 (1), 5–17.

Shur, Y.L., Jorgenson, M.T., 2007. Patterns of permafrost formation and degradation in relation to climate and ecosystems. Permafr. Periglac. Process. 18, 7–19. https://doi.org/10.1002/ppp.582.

Smith, S.L., Romanovsky, V.E., Lewkowicz, A.G., Burn, C.R., Allard, M., Clow, G.D., Yoshikawa, K., Throop, J., 2010. Thermal state of permafrost in North America: a

contribution to the international polar year. Permafr. Periglac. Process. 21, 117–135. https://doi.org/10.1002/ppp.690.
Smith, S.L., Riseborough, D.W., Bonnaventure, P.P., 2015. Eighteen year record of forest fire effects on ground thermal regimes and permafrost in the Central Mackenzie Valley, NWT, Canada. Permafr. Periglac. Process. 26 (4), 289–303.
Spence, C., Woo, M.-K., 2003. Hydrology of subarctic Canadian shield: soil-filled valleys. J. Hydrol. 279, 151–156.
Stoof, C.R., Wesseling, J.G., Ritsema, C.J., 2010. Effects of fire and ash on soil water retention. Geoderma 159, 276–285. https://doi.org/10.1016/j.geoderma.2010.08.002.
Thompson, D.K., Waddington, J.M., 2013. Wildfire effects on vadose zone hydrology in forested boreal peatland microforms. J. Hydrol. 486, 48–56. https://doi.org/10.1016/j.jhydrol.2013.01.014.
Tjerngren, I., Karlsson, T., Björn, E., Skyllberg, U., 2012. Potential Hg methylation and MeHg demethylation rates related to the nutrient status of different boreal wetlands. Biogeochemistry 108 (1–3), 335–350. https://doi.org/10.1007/s10533-011-9603-1.
Toride, N., Leij, F.J., van Geuchten, M.Th., 1995. The CXTFIT code for estimating transport parameters from laboratory or field tracer experiments, Version 2.0. U. S. Department of Agriculture, U. S. Salinity Laboratory Agricultural Research Service. Report 137.
U.S. EPA, Method 1630, 1998. Methyl Mercury in Water by Distillation, Aqueous Ethylation, Purge and Trap, and Cold Vapor Atomic Fluorescence Spectrometry. U.S. Environmental Protection Agency, Washington, D.C.
U.S. EPA, Method 1631, 2002. Revision E: Mercury in Water by Oxidation, Purge and Trap, and Cold Vapour Atomic Fluorescence Spectrometry. U.S. Environmental Protection Agency, Washington, D.C.
U.S. EPA, Method 200.7, 1994. Determination of Metals and Trace Elements in Water and Wastes by Inductively Coupled Plasma-atomic Emission Spectrometry. U.S. Environmental Protection Agency, Washington, D.C.
U.S. EPA, Method 300.1, 1997. Determination of Inorganic Anions in Drinking Water by Ion Chromatography. U.S. Environmental Protection Agency, Washington, D.C.
Waddington, J.M., Morris, P.J., Kettridge, N., Granath, G., Thompson, D.K., Moore, P.A., 2015. Hydrological feedbacks in northern peatlands. Ecohydrology. https://doi.org/10.1002/eco.1493.
Walvoord, M., Kurylyk, B., 2016. Hydrologic impacts of thawing permafrost - a review. Vadose Zone J. 15 (6). https://doi.org/10.2136/vzj2016.01.0010.
Warren, R.K., Pappas, C., Helbig, M., Chasmer, L.E., Berg, A.A., Baltzer, J.L., Quinton, W.L., Sonnetag, O., 2018. Minor contribution of overstory transpiration to landscape evapotranspiration in boreal permafrost peatlands. Ecohydrology 11, 1975.
Whittington, P.N., Price, J.S., 2006. The effects of water table draw-down (as a surrogate for climate change) on the hydrology of a fen peatland, Canada. Hydrol. Process. 20, 3589–3600.
Wotton, B.M., Nock, C.A., Flannigan, M.D., 2010. Forest fire occurrence and climate change in Canada. Int. J. Wildland Fire 19 (3), 253–271.
Wotton, B.M., Flannigan, M.D., Marshall, G.A., 2017. Potential climate change impacts on fire intensity and key wildfire suppression thresholds in Canada. Environ. Res. Lett. 12, 095003.
Wright, N., Hayashi, M., Quinton, W.L., 2009. Spatial and temporal variations in active layer thawing and their implication on runoff generation in peat-covered permafrost terrain. Water Resour. Res. 45 (W05414), 1–13. https://doi.org/10.1029/2008WR006880.
Yoshikawa, K., Bolton, W.R., Romanovsky, V.E., Fukuda, M., Hinzman, L.D., Bolton, W.R., Romanovsky, V.E., Fukuda, M., Hinzman, L.D., 2001. Impacts of wildfire on the permafrost in the boreal forests of interior Alaska. J. Geophys. Res. 108 (D1). https://doi.org/10.1029/2001JD000438.
Zoltai, S.C., Tarnocai, C., 1975. Perennially frozen peatlands in the Western Arctic and subarctic of Canada. Can. J. Earth Sci. 12, 28–43. https://doi.org/10.1139/e75-004.